Turbulence Transport Modelling in Gas Turbine Related Applications

ANDREAS SVENINGSSON

Department of Applied Mechanics
CHALMERS UNIVERSITY OF TECHNOLOGY
Göteborg, Sweden, 2006

THESIS FOR THE DEGREE OF DOCTOR OF PHILOSOPHY IN
THERMO AND FLUID DYNAMICS

Turbulence Transport Modelling in Gas Turbine Related Applications

ANDREAS SVENINGSSON

Department of Applied Mechanics

CHALMERS UNIVERSITY OF TECHNOLOGY

Göteborg, Sweden, 2006

Turbulence Transport Modelling in Gas Turbine Related Applications

Andreas Sveningsson
ISBN 91-7291-739-3

Ny serie nr 2421
ISSN 0346-718X

Department of Applied Mechanics
Chalmers University of Technology
S-412 96 G¨oteborg, Sweden
Phone +46-(0)31-7721400
Fax +46-(0)31-180976

This document was typeset using LaTeX.

Printed at Chalmers Reproservice
G¨oteborg, Sweden

Turbulence Transport Modelling in Gas Turbine Related Applications

Andreas Sveningsson

Division of Fluid Dynamics
Department of Applied Mechanics
Chalmers University of Technology

Abstract

Computational fluid dynamics is a cornerstone in gas turbine engine design. It is used to optimize shapes of turbine and compressor airfoils, to predict heat transfer to gas turbine hot parts, to reduce the amount of pollutants that form when fuel is burnt, to reduce gas turbine noise and so on. There are still, however, areas where the computational methods lack in reliability and need further refinement. One is the modelling of turbulence transport effects on mean flow characteristics and is the main subject of this thesis. The thesis focuses on RANS predictions of turbulence and heat transfer, where the unknown turbulence transport terms are closed using turbulence models based on the eddy-viscosity concept.

The potential of using the $v^2 - f$ turbulence model for heat transfer predictions in complex flows is illustrated by computing a three-dimensional stator vane passage flow. It is shown that the $v^2 - f$ model is able to predict the effects of turbulence on the secondary flow field in the stator passage, and, that the secondary flow field is largely what determines the heat transfer to the vane endwalls. The use of the realizability constraint to prevent unphysical growth of turbulence kinetic energy is also thoroughly discussed.

There are however problems with the $v^2 - f$ model as well. It is in principle unable to resolve turbulence anisotropy and furthermore suffers from predicting laminar to turbulent boundary layer transition too rapidly. It is shown that the former problem can be dealt with by employing the nonlinear eddy-viscosity model of Pettersson-Reif (2000). This model is tested in the asymmetric diffuser flow and proves to be capable of very accurate Reynolds stress predictions. This study also highlights the strong sensitivity of the mean flow to turbulence closure and suggests that the near wall modelling is of the utmost importance. In an effort to improve the performance of the $v^2 - f$ model in transitional flows the ideas behind the transition modelling approach of Walters & Leylek (2004) are adapted to the $v^2 - f$ model. Also provided is an overview of the existing literature on the subject of transition modelling.

Keywords: RANS, V2F, realizability, transition, secondary flow, heat transfer

List of Publications

This thesis is based on the work contained in the following papers:

- A. Sveningsson and L. Davidson, 2004, Assessment of Realizability Constraints in $\overline{v^2} - f$ Turbulence Models, *International Journal of Heat and Fluid Flow*, 25, 785-794

- A. Sveningsson and L. Davidson, 2005, Computations of Flow Field and Heat Transfer in a Stator Vane Passage Using the $\overline{v^2} - f$ turbulence model, *ASME Journal of Turbomachinery*, 127, 627-634

- A. Sveningsson, B. A. Pettersson-Reif and L. Davidson, 2005, Modelling the Entrance Region in a Plane Asymmetric Diffuser by Elliptic Relaxation, Submitted to International Journal of Heat and Fluid Flow

- A. Sveningsson, 2005, Transition Modelling–A Review

- A. Sveningsson, 2005, Towards an Extension of the $v^2 - f$ Model for Transitional Flows

Division of Work Between Authors

The respondent is the first author of all papers on which this thesis is based, and the respondent produced all the results.

In the work described in Papers I-II the numerical computations were performed with an in-house code, parallelized by Dr. Håkan Nilsson. The respondent implemented the different versions of the $v^2 - f$ model and the coupled TDMA solver used in these studies. The work of a theoretical nature on the effect of the realizability constraint was carried out by the respondent and discussed with Professor Lars Davidson.

In Paper III most of the modifications to the nonlinear $v^2 - f$ model were suggested by Anders Pettersson-Reif, who at an early stage believed that the poor

modelling performance could be improved by modifying the dissipation rate equation. The respondent carried out most of the analysis of the results, which was energetically discussed with the coauthors. All implementations were made by the respondent.

The work described in Papers IV-V was mainly performed by the respondent. Lars Davidson provided valuable comments throughout the process.

Other Relevant Publications

- A. Sveningsson, B. A. Pettersson-Reif and L. Davidson, 2005, Modelling the Entrance Region in a Plane Asymmetric Diffuser by Elliptic Relaxation, In: *Proceedings of the Fourth International Symposium on Turbulence and Shear Flow Phenomena*, vol 3, 1183-1188, Williamsburg, USA

- A. Sveningsson, 2003, Analysis of the Performance of Different $\overline{v^2} - f$ Turbulence Models in a Stator Vane Passage Flow, Licentiate Thesis, *Division of Thermo and Fluid Dynamics, Chalmers University of Technology, Gothenburg*

Acknowledgements

There are several persons without whom this thesis would probably never have been written. My supervisor, Professor Lars Davidson, must of course be first in line. Without his encouragement and belief in me as a research student I would not have gotten past the licentiate degree. I am also deeply grateful for all the hours that Lars has spent critically reading my manuscripts, which has certainly improved their quality. Thanks also to my co-supervisor, Dr. Håkan Nilsson, for teaching me how to CALC and for helping me with all ICEM pitfalls.

I would also like to express my gratitude to Dr. Anders Petterson-Reif. The work behind Paper III and the nonlinear model would not have been carried out without his devoted support. His appearence at the Department also boosted my motivation to continue my studies.

I must also mention Docent Gunnar Johansson and Professor Bill George who have done their best to teach me fractions of what they know about fluid dynamics in general and turbulence in particular. They have also served as good examples of fluid dynamics researchers.

Professor Karen Thole, at the Virginia Polytechnic Institute and State University, is also gratefully acknowledged for instantly supplying experimental data whenever needed.

Special thanks also to Dr. Jonas Larsson at Volvo Aero Corporation for all instruction when I was learning Fluent and for letting me use the computer facilities at VAC at the beginning of this project.

The financial and gas turbine technological support of the partners involved in the Swedish Gas Turbine Center (GTC) is gratefully acknowledged. Special thanks go to Esa Utriainen for his keen interest in my work and to Sven Gunnar Sundkvist for the superb management of GTC, from which I learned quite a lot.

Finally, Eva is the oustandingly most important person to this thesis (and not only the thesis!). Life is easy with You by my side.

A.S.

Göteborg
January, 2006

Nomenclature

Latin Symbols

C	true vane chord; turbulence model constant
C_{lim}	constant in the realizability constraint
f	relaxation parameter
k	turbulent kinetic energy, defined as $k = \frac{1}{2}\overline{u_i u_i}$
L	turbulent length scale
P	vane pitch
P_ϕ	production rate of ϕ
p	pressure
S	vane span; source term; $S^2 = S_{ij}S_{ij}$
S_{ij}	mean strain rate tensor, $S_{ij} = \frac{1}{2}\left(\frac{\partial U_i}{\partial x_j} + \frac{\partial U_j}{\partial x_i}\right)$
St	Stanton number, defined as $h/\rho C_p U_{in}$
$\mathcal{T}$	turbulent time scale
U	mean velocity in x-direction
U_i	mean velocity in x_i-direction
u	fluctuating velocity in x-direction
u_i	fluctuating velocity in x_i-direction
$\overline{u_i u_j}$	Reynolds stress tensor
V	mean velocity in y-direction; secondary velocity; volume
$\mathcal{V}$	turbulent velocity scale
v	fluctuating velocity in y-direction
v^2	turbulence velocity scalar
W	mean velocity in z-direction
w	fluctuating velocity in z-direction

Greek Symbols

δ	boundary layer thickness
δ_{ij}	Kronecker delta
ε	dissipation rate
ε_{ijk}	alternating unit tensor
η	efficiency
λ	eigenvalue of strain rate tensor
μ	dynamic viscosity
μ_t	dynamic turbulent viscosity
ν	kinematic viscosity
ν_t	kinematic turbulent viscosity
ρ	density
σ_Φ	turbulent Prandtl number for variable Φ
ϕ	fluid propoerty; pressure-strain rate
ω_i	vorticity component in x_i-direction

Subscripts

in	inlet
E	east
e	external
W	west
w	wall

Abbreviations

BFC	Boundary Fitted Coordinates
DNS	Direct Numerical Simulation
GGDH	General Gradient Diffusion Hypothesis
LES	Large-Eddy Simulation
LKE	Laminar Kinetic Energy
RANS	Reynolds Averaged Naviers-Stokes
SMC	Second Moment Closure
TDMA	Tri-Diagonal Matrix Algorith
TKE	Turbulence Kinetic Energy
UDF	User-Defined Function

Contents

Chapter 1

Introduction

1.1 Motivation

Consider the flow in a breath of air, the mixing of milk in a cup of coffee, the flow behind any airborne animal or man-made object, the smoke exiting a chimney, the air on the leeward side of a poorly set sail, the water whirls in rills or rivers, or even the Gulf Stream, the fascinating winds in hurricanes and our ever-changing weather system. They, and the vast majority of all other fluid flows, have one thing in common–they are all of a turbulent nature. Before continuing it is necessary to discuss what is meant by a flow being turbulent, or perhaps equally important, not turbulent. Trying to explain the differences of a turbulent flow and a nonturbulent flow, hereafter referred to as a laminar flow, in words is useless. Consider instead the two pictures in Figure 1.1. The laminar flow in the jet to the left consists of fluid layers (cylinders) that slide along each other as the jet passes smoothly by. Initially the laminar jet is completely stable but at some distance downstream the jet exit it becomes unstable and begins to form large regular vortices that entrain surrounding fluid, which enhances the mixing and spreading of the jet. The fluid motion seen in Figure 1.1b is very different from that in the laminar jet. It consists of three-dimensional, irregular motions of fluid elements, usually referred to as eddies, of varying size and intensity. These eddies are characteristic of turbulence.

A most important feature of turbulent flows, as compared with laminar ones, is that these flows have extremely good mixing properties. Consider for example the careful pouring of one liquid into another, e.g. milk in coffee. The two fluids will of course be mixed to some extent but the process is fairly slow, especially if the initial fluid motion ceases and all transport takes place on a molecular level. If then the mixture is stirred with a spoon the two fluids will almost instantly mix. This is

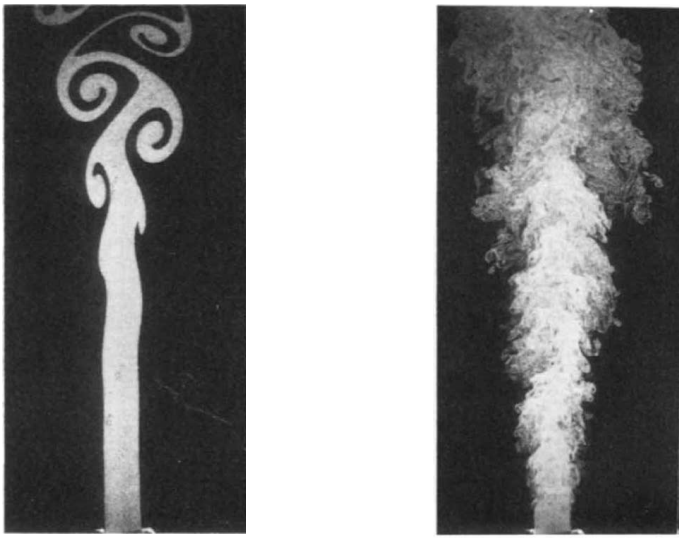

(a) $Re = 330$ (b) $Re = 4520$

Figure 1.1: Two photos illustrating the fundamental difference between laminar and turbulent flows. The (white) jet fluid is exiting in a surrounding at rest. Reprinted with permission from S. Gogineni, C. Shih, and A. Krothapalli, the Gallery of Fluid Motion 1993, Paper S6. Copyright 1993, American Institute of Physics.

due to the creation of three-dimensional irregular motions on a scale much larger than the molecular level, i.e. turbulence. The turbulent motions have the potential to rapidly transport fluid particles over relatively large distances and should be compared with the random process of molecular motions on a far smaller scale. In flows where it is difficult to create turbulence, e.g. if we are to carefully mix two buckets of viscous paint, the mixing process will be significantly slower. We thus understand that if we are interested in a fluid flow's mixing properties it is of crucial importance that the effects of turbulence are included.

This project doesn't at all deal with paint mixing resulting from turbulence. The question is rather how turbulence mixes a fluid of high temperature with a fluid of lower temperature and a fluid of high momentum (velocity) with a fluid of low momentum (velocity). The reader is probably wondering why this should be so difficult. Aren't there fundamental laws that describe the physics of fluid motion (and turbulence)? There are, but the problem is that this set of equations, given in their most general form, which is indeed needed to describe turbulence, in highly nonlinear and cannot be solved analytically. Why then, the reader might think, can't we use all the fancy methods of numerical analysis, discretize and

solve the governing equations in an approximate manner and make sure that the errors in the approximation are negligible? This is in fact exactly what an increasing part of the turbulence research community is doing and is referred to as Direct Numerical Simulations (DNS). There is however a problem with DNS of turbulent flows. The problem is that every single eddy of the flow, no matter how small, must fit in the numerical grid. Consider again the turbulent jet depicted in Figure 1.1b. A fair requirement on resolution of this flow would be that the very smallest structures seen in the picture should be covered by, say, three to five grid points in all three geometrical dimensions. Johansson & Klingmann (1994) made measurements of the smallest scales present in a $1cm$ wide air jet ($\nu \sim 10^{-5}$) with an exit velocity of $10m/s$ ($Re \approx 7000$) and found that their sizes were in the order of $0.1mm$, i.e. a size comparable to the thickness of a hair, at about 20 jet widths downstream of the exit. If we then assume that we need to store data at three positions across these structures in a computational domain with a $0.1 \times 0.1m$ cross section that is, say, $1m$ long, we end up with approximately $3000 \times 3000 \times 30000 \approx 10^{11}$ computational points. The largest meshes of today contain on the order of 10^8 points and we can thus understand that a fully resolved DNS of the described jet will not be realistic for a long time[1]. In the meantime we will somehow have to model the effect of at least the smaller turbulent motions. This modelling, i.e turbulence modelling, is primarily what this project is about.

Turbulence modelling results in models of turbulence that are approximations of real physics. Regardless of the accuracy of these models they can, with varying degree of difficulties in properly defining the problem, be applied to any turbulent fluid flow. Generally speaking, one may say that the cruder the model approximations the easier the model is to use. It shall therefore come as no surprise that some of the most popular turbulence models of today are not very sophisticated and are being used in applications that they were not first designed for. Surprisingly enough, however, these models, in the hands of an experienced user, often produce useful results in a wide variety of complex flows.

One area in which turbulence models of varying complexity are being extensively used is the design of gas turbine engines. This field also contains the applications for which the model development presented in this thesis are intended. In turbine parts of gas turbine engines one of the most crucial shortcomings of

[1]Note that the ratio, R, of the largest turbulent structures, comparable to a chacteristic physical length scale, e.g. the width of the jet, to the smallest turbulent structures depends on the Reynolds number, $Re = uL/\nu$, as $R \sim Re^{-3/4}$. Thus, for typical industrial applications, where the Reynolds number is often one to two orders in magnitude larger and the geometry is much more complex, the requirements on resolution is even worse. Note also that the DNS requirement of time resolution, which is equally severe as the space resolution requirement, has been omitted in the present discussion.

turbulence models is their inability to give reliable predictions of the effect of turbulence transport of heat (i.e. the mixing of hot and cold fluids). The following section highlights the importance to these machines of accurately accounting for heat transfer due to turbulence Of equal importance to the overall efficiency of gas turbine engines are accurate predictions of momentum transport due to turbulence (the mixing of high and low speed fluids). If the effects of momentum traqnsport cannot be accounted for correctly, computations that overpredict it may suggest too aggressive designs and lead to great reductions in stage efficiency owing to large separated regions. Another consequence would be overpredictions of skin friction losses, which account for about half the loss in stage efficiency of a compressor stage (at its design point).

1.2 The Influence of Temperature on Gas Turbine Performance

The inventors of gas turbine engines were not very concerned about the efficiency of their machines. They were happy with the fact that their devices were able to transform the internal energy of a fuel into mechanical power output, and the cost of the fuel at that time was probably not an issue. As every car owner of today knows, that situation has changed quite dramatically. The fuel price is all but low and even the smallest increase in performance can lead to decisive differences when the gas turbine cost-effectiveness is compared with that of the products of competing manufacturers.

The ever increasing efficiency of gas turbines lies today in the range of 35-40%, which of course is a significant improvement since the early days of gas turbine technology. The prospects of further improvements can be illustrated by analyzing a real gas turbine using the Brayton cycle, which is the ideal thermodynamic cycle for gas turbines. The efficiency of this cycle, η, is

$$\eta = 1 - \left(\frac{P_{low}}{P_{high}} \right)^{\gamma/(\gamma-1)} \tag{1.1}$$

where $\gamma > 1$ is a constant and P_{high} and P_{low} are the high and low pressure levels in the ideal cycle. We thus see that the only way to increase the efficiency is to either lower P_{low} or raise P_{high}. As P_{low} is coupled to the pressure of the engine surroundings we must raise P_{high} in order to increase the efficiency of the gas turbine. Note that there is no explicit temperature dependence present in the efficiency expression of the Brayton cycle. Nevertheless the temperature of the gas entering the (gas) turbine has increased quite dramatically over the last

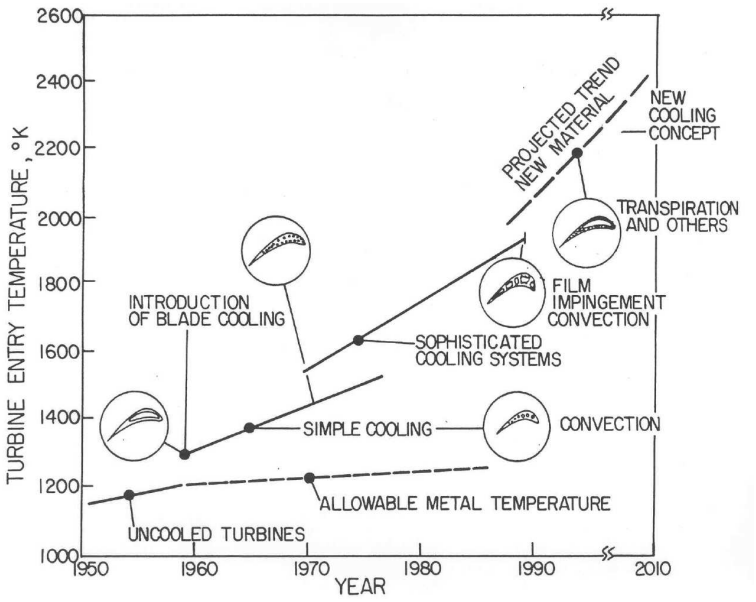

Figure 1.2: Development of gas turbine inlet temperature illustrating the impact of cooling technology.

decades as illustrated in Figure 1.2. What then, if not an increase in performance, is the reason for this rise in temperature? In Figure 1.3 the effect of turbine inlet temperature on the performance and specific output (net work output per unit mass flow rate) of a more realistic gas turbine is illustrated. Here a model of a simple cycle gas turbine[2] is analyzed and it can be seen that the efficiency, and especially the specific output, increases with increased inlet temperature. Even if the improved efficiency in this cycle is not negligible it is the increase in specific output that has been the driving force towards higher temperatures. The benefit from an increased specific output is for stationary gas turbines (power plants) simply that a specific engine produces more power as the temperature increases and for aircrafts that big (heavy) engines may be replaced by smaller ones to increase the payload. The major problem in further increasing the temperatures in a gas turbine is that the rise in temperature will increase the heat load on the hot parts of the gas turbine. This increases the thermal stresses in the gas turbine material and shortens its lifetime.

An interesting observation can be made in Figure 1.2, which shows the influence of blade cooling on the inlet temperature of the turbine. Without cooling, the turbine's maximum allowable inlet temperature is restricted by the temperature of

[2]Isentropic compressor and turbine effi ciency of 0.8 and 0.85, respectively.

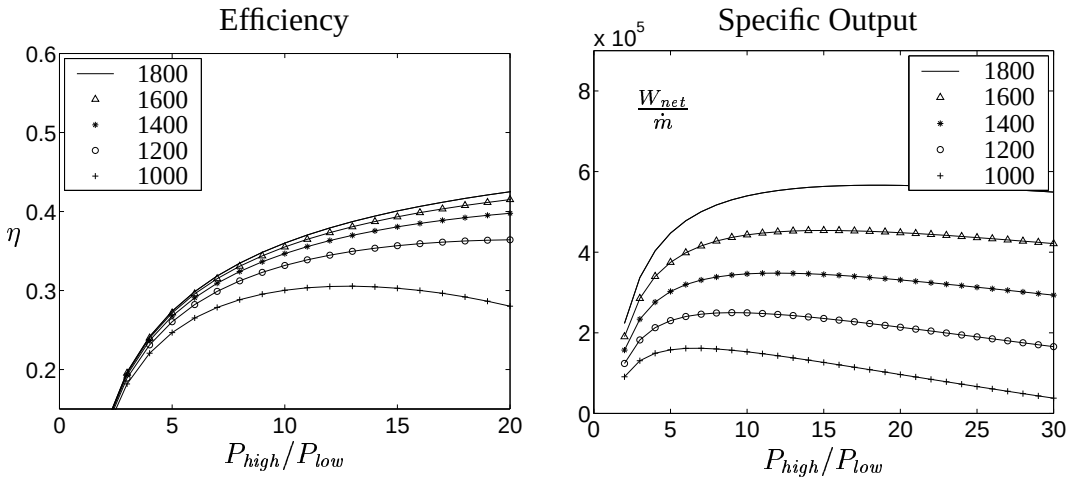

Figure 1.3: The relation of gas turbine efficiency and specific output to compression ratio and turbine inlet temperature (degree Kelvin).

the gas turbine's hot parts, where the material they are made of begins to lose its structural properties and can no longer withstand the thermal or pressure induced stresses mentioned above. The figure has a line that shows the effect of inventing new materials with better high temperature properties on the allowable turbine inlet temperature. This effect must be compared with that of cooling. Clearly, neither of the two approaches to increasing the temperature in gas turbines can be neglected but, when compared, it becomes evident that *the potential of lowering the temperature of the hot parts is higher than increasing the highest allowable hot part temperature*. Hence, in order to prolong the life cycle of gas turbines, or to increase their performance, the most efficient route is likely to further develop the turbine cooling technology. For example, reducing the mean section temperature of a rotor blade by 15^oC would approximately double its lifetime expectancy.

However, there is also a problem with cooling. Supplies of coolant are by no means free. It has to be by-passed from the gas turbine compressor, and the more coolant removed from the main flow path the lower the overall efficiency. Further, the pressure is very high at the locations of the gas turbine where the most cooling is needed, i.e. in the combustor and the first stator/rotor stage. Thus, for coolant to enter these areas at all it must be by-passed from the very latest stages of the compressor, where it is the most expensive. Therefore, the by-passed coolant must be used as efficiently as possible, which also couples the design of the cooling system with the choice of operating temperature. In other words, there is a trade-off temperature at which further increases in temperature require amounts of coolant that cannot be justified from an efficiency point of view.

Improving gas turbine cooling is all but a trivial matter and requires a thorough understanding of how the complex flow field in the combustor and the first stator/rotor stage develops. For example, the external gas path flow determines the optimal locations for the injection of coolant. That is, these locations should idelly be chosen such that most of the injected fluid remains close to the parts exposed to the hottest flow conditions. The thermal load on the turbine is particularly important as the first stator vanes are hit by an accelerated, very hot and highly turbulent stream of gas causing high heat transfer rates in the stagnation region of the vanes. Another complicating factor is that the conditions around turbine airfoils (i.e. stator vanes or rotor blades) strongly influence the state of the boundary layer. That is, even though the free stream downstream of the combustor is highly disturbed, the strong acceleration around the airfoils makes it difficult to tell whether the airfoil boundary layer will be of a laminar, turbulent or transitional nature. Keeping the mixing properties of turbulence discussed in the previous section in mind it should come as no surprise that the heat transfer rates in a turbulent boundary layer can reach levels several hundred percent higher than those in laminar boundary layers. Therefore, numerical methods aimed at facilitating the design of the next generation of gas turbines engines must be able to accurately account for the effect of turbulent transport on complex free stream flow structures and boundary layer heat transfer and must thus also be able to determine the state of boundary layers.

1.3 The Need for Endwall Cooling

The previous section argued that an efficient way to increase the performance of gas turbines is to increase the temperature of the gas exiting the combustor. It was also shown that this temperature has indeed increased substantially over the last decades. Further, it was mentioned that the increase in temperature causes the heat transfer to the turbine airfoil to grow significantly. This is nothing new and, as heat transfer to turbine blades has been studied thoroughly, it is fairly well understood what is required to keep the temperature of the airfoil surfaces sufficiently low. Typically, most of the coolant is injected in the vicinity of the leading edge and remains close to the blade throughout the blade passage as the flow around the blade is, at least when the turbine is operated at design conditions, essentially two-dimensional and attached to the blade surface. Recently, however, as energy consumption is continuously growing, increased environmental awareness has led to legislated requirements for reduced levels of pollutants from energy power plants. A consequence of this is the trend of using so called low NO_x burners, which substantially reduce the exhaust levels of NO_x. The

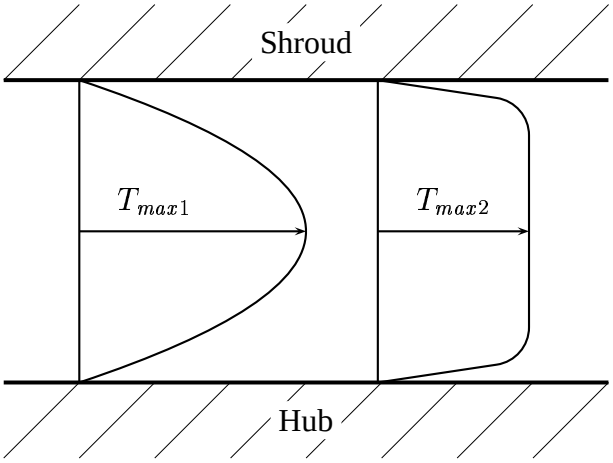

Figure 1.4: Schematic illustration of the trend towards flatter inlet temperature profiles and higher thermal loads on gas path endwalls.

working principle of these burners is to reduce the maximum temperature in the combustor, as most of the NO_x forms in high temperature regions. A reduction in temperature however contradicts the increase needed to improve gas turbine performance. The only solution that meets both these requirements is to even out the turbine inlet temperature profile as illustrated in Figure 1.4. Both temperature profiles seen are about the same on average, but the maximum temperature in the right profile is significantly lower than that of the left profile. Consequently, the energy content (gas temperature) of the flow in the vicinity of the endwalls must be larger in the profile to the right. As the allowable endwall temperatures are the same in both cases this implies larger cross-stream temperature gradients towards the endwalls and thus higher rates of heat transfer to the endwalls. The only way to prevent this increase is to also inject coolant along the gas path endwalls. This is the main reason for the recent increase in interest in the flow and heat transfer in the endwall region of gas turbines. In the next section we will see that injecting coolant to protect gas turbine endwalls is not straightforward.

1.4 Gas Turbine Secondary Flow Field Structures

1.4.1 A Secondary Flow Mechanism

Consider the velocity profile downstream of the combustor entering the first stator vane passage. The friction along the combustor walls, and the duct connecting the

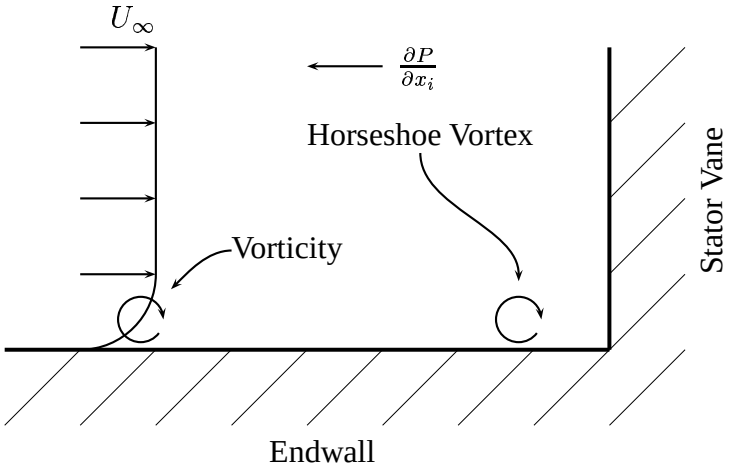

Figure 1.5: Illustration of the (inviscid) mechanism behind the generation of secondary flow structures in the vane/endwall junction. The pressure gradient decelerates the freestream flow as the vane stagnation is approached. The vorticity in the oncoming boundary layer on the other hand remains unaffected by the pressure gradient and is the origin of the horseshoe vortex system.

combustor and the vane passage, has generated vorticity that enters the vane passage in the form of a boundary layer[3]. As the boundary layer approaches a stator vane stagnation point, where the velocity by definition should reduce to zero, it is affected by a pressure gradient. The magnitude of the adverse pressure gradient is largely determined by the freestream velocity with which the gas approaches the vane (as the pressure gradient must be large enough to reduce this velocity to zero at the stagnation point) and is of a 'nonlocal' nature. Due to its nonlocality the pressure gradient decelerates the slowly moving boundary layer fluid just as much as the freestream fluid, which reverses the flow in the near wall region and causes a recirculating flow region to appear. This process is illustrated in Figure 1.5. A perhaps more direct way to draw the same conclusion is to look at the vorticity equation. This equation doesn't involve a pressure gradient term, and thus the vorticity in the boundary layer cannot be affected by the above mentioned adverse pressure gradient. In fact, the same equation shows that vorticity cannot be affected by body forces (such as the pressure) acting through fluid particle centers of mass, but only through shearing forces (such as the friction force on the vane passage endwalls). Therefore, the vorticity that has entered the boundary

[3]The shearing motion in the boundary layer may be viewed as a superposition of a straining motion and a rigid rotation (c.f. Batchelor, 1967).

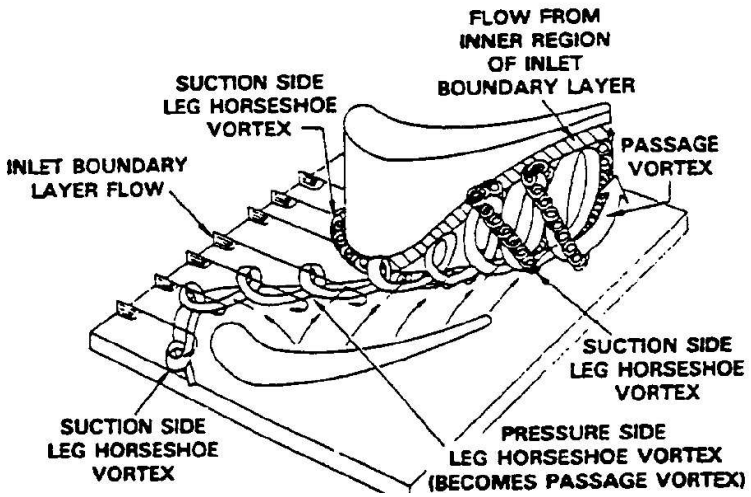

Figure 1.6: Secondary flow model by Sharma & Butler (1987).

layer through the endwalls is conserved and, when it cannot be convected past the stator vane, it results in a so called horseshoe vortex.

The nature of horseshoe vortices has been studied rather extensively in a variety of geometries where a boundary layer is blocked by an object of finite lateral thickness, e.g. a cube or a turbine airfoil. An example is the study by Sharma & Butler (1987) who measured the secondary flow within a turbine airfoil passage. They identified the above mentioned horseshow vortex and followed its evolution in the highly curved flow field through the vane passage. Their findings led to the secondary flow model shown in Figure 1.6. As can be seen, the flow is complex. Its most important contents are the horseshoe vortex, with one pressure side leg and one suction side leg, and the so called passage vortex. The term passage vortex is in the author's opinion unfortunate as its appearence is caused by the same mechanism as the pressure side leg of the horseshoe vortex, i.e. the vorticity in the endwall boundary layers. In other words, the term passage vortex is redundant and somewhat confusing. Also present are smaller structures, e.g. corner vortices, caused by the boundary layers (vorticity) that develop along the airfoil surface in the downward moving portion of the horseshoe vortex roll-up (cf. Sveningsson & Davidson, 2005).

After the rotating motion has formed it is convected through the passage and experiences the difference in pressure of the pressure and suction sides of two adjacent vane profiles. It is this pressure gradient that makes the flow turn as it passes through the vane passage (strictly speaking, it is vice versa, i.e. the *profile* forces the flow to turn and the associated acceleration is the reason for the

pressure difference). The flow turning makes the fluid experience a centripetal force. This force is greater the higher the velocity of the curved flow. Thus, the fluid close to the endwall, which contains slightly less momentum than fluid in the freestream, tends to change direction more rapidly than fluid away from the wall. The consequence is that the pressure side leg of the horseshoe vortex moves towards the suction side. This is illustrated in Figure 1.6.

1.4.2 The Influence of Secondary Flows on Heat Transfer

The complex structure of the secondary flow in the gas passage is of great interest in its own right. But let us now return to the problem of cooling the turbine endwalls, or more precisely, endwall cooling under the influence of the secondary flow depicted above. Consider a boundary layer into which 'insulating' coolant has been injected to protect the endwall from the hot freestream gas, approaching a stator vane. At the location of the horseshoe vortex roll-up, the boundary layer (containing the added coolant) will separate from the endwall surface, which here becomes exposed to the hot gases of the freestream. That is, downstream of the point of separation the efforts spent to cool the endwall surface are more or less wasted. Recall also the trend of flattening the inlet temperature profiles, which produces thin thermal boundary layers. As these layers are thin, only a small amount of vorticity is needed to bridge the endwall surface at the stagnation point with the high temperature freestream fluid.

To aid the understanding of this heat transfer mechanism, consider the visualization of the horse shoe vortex/endwall heat transfer interaction in Figure 1.7. The results are from a $v^2 - f$ model computation (cf. Sveningsson & Davidson, 2005) of the low freestream turbulence intensity test case described and experimentally studied by Kang & Thole (2000). The blue body is a stator vane and the endwall is colored by its temperature. Note that here the 'real' problem is reversed. That is, the endwall is heated and the freestream fluid cools the endwall. The location of separation is illustrated by the black friction lines plotted on the surface of the endwall, which clearly show the presence of a saddle point. Immediately beyond the imaginable line of separation the surface heat transfer increases drastically. This is due to the fact that the thick thermal boundary layer separates from the endwall, which in turn allows room for freestream fluid to come into contact with the endwall. Note that the thermal layer is initially very thin and that the longer the developing boundary layer remains attached to the endwall the weaker is the heat transfer. The blue streamlines show the center of the horseshoe vortex whereas the white lines illustrate the downwash of cold freestream fluid in the stagnation region that strongly affects the endwall heat transfer rate.

Understanding this type of flow is important in turbomachinery design. For

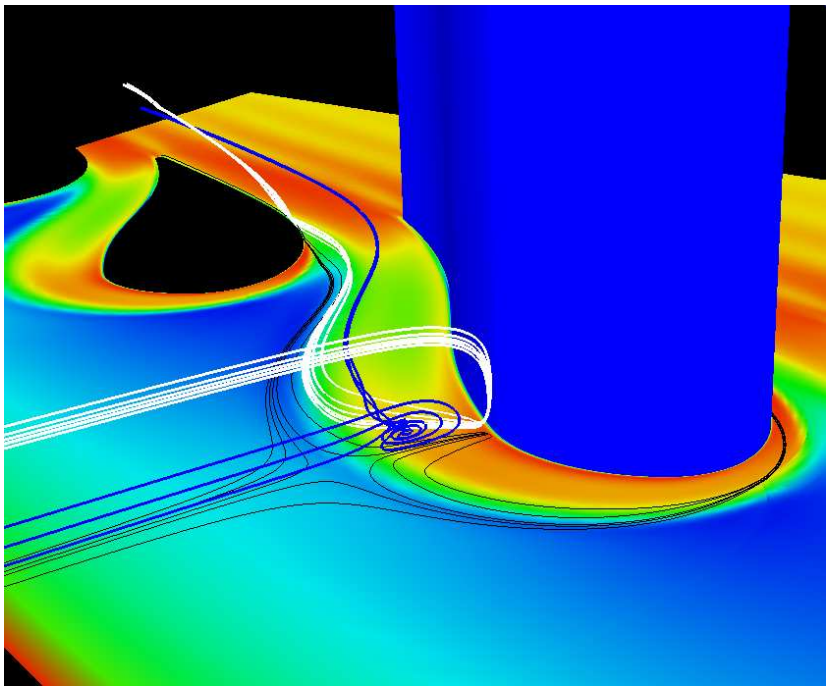

Figure 1.7: Visualization of the endwall heat transfer enhancement caused by the presence of secondary flow structures. The blue body is a stator vane. The constant heat flux endwall is colored by its temperature (red is cold, blue is hot). The blue and white streamlines show the center of the horseshoe vortex pressure side leg and the downwash of cold freestream fluid that cools the endwall, respectively. The black wall friction lines illustrate the sadde point being formed as a result of the horseshoe vortex roll-up.

example, any attempt to design an effective cooling of the endwall must take into account the fact that the vortices will lift an ejected insulating cool air film away from the endwall material it is supposed to protect. In such a case the only effect the coolant will have is to lower the average temperature of the vane passage fluid, i.e. to decrease the efficiency of the turbine. To help our understanding it is highly desirable to have accurate computational methods that conveniently allow parametric studies of the influence of geometry, blade loading, freestream turbulence, different cooling concepts, blade counting, inlet flow boundary conditions and so on. The alternative is to perform each such investigation experimentally, which is expensive. Unfortunately, computations resolving all the flow scales that are present are still beyond our scope and we are back at the problem raised in the first section–*how can we model the influence of turbulent fluctuations?*

1.4.3 Relevant Past Studies

For the last fifty years an enormous amount of research has been invested in the area of gas turbine technology. As discussed in the previous chapter the driving force has been requirements for high efficiency and low emissions. The literature on the subject is vast. The main reason is of course that the subject is very difficult, as almost all the features that make the life of a fluid mechanist hard are present. Some examples are heat transfer itself (which is very difficult both to measure and compute), three-dimensional flow fields, unsteady interactions between stator and blade rows, high temperatures and pressures, transition, strong compressibility effects, high freestream turbulence intensities, streamline curvature, the need for addition of cooling and so on.

In the world of gas turbine research (as in most other worlds) the standard approach is to try to separate as many of these effects as possible from each other and study them individually. One disadvantage is that, when dealing with fluid flows, it is difficult to tell what effects *can* be investigated individually. An example from this project could be whether is it relevant or not to draw any conclusions from a CFD analysis on how the secondary flow field distributes film cooling air if the film cooling itself is not included in the analysis. Another problem is that the research area gets split up in many subareas, which makes it difficult to give an overview of the present research status. Nevertheless, a few studies that highlight the effect of secondary flows on heat transfer are given below. As the heat transfer to endwalls and its dependence on secondary flow structures are of particular interest in this project, the focus is on studies that include both the flow adjacent to turbine endwalls and the heat transfer to the same.

Measurements and Predictions of Gas Turbine Heat Transfer and Flow Field

Much of today's understanding of the turbine gas path flow field and heat transfer stem from experiments carefully conducted during the later decades of the 20th century. These experiments not only provide the basic understanding of the underlying flow physics but also form a growing data set that can be used to validate the performance of numerical predictions.

The earliest review of the subject is the paper by Sieverding (1985) that summarizes the status of experimental secondary flow research of the time. Of special interest is the discussion of the development of endwall flow models and the physics behind the horseshoe vortex system. One of the conclusions is that the properties of the complex set of vortices depend on the stator vane geometry and that the leading edge effects are closely related to the incidence angle, which suggests variations in the secondary flow field at off design conditions.

Eight years later Simoneau & Simon (1993) made a review of the state of the art in three related areas: configuration specific experiments, fundamental physics and model development, and code development. All these areas are claimed to be needed to develop accurate predictive tools for heat transfer in turbine gas paths. A contribution believed to be among the most important is the rotating rig research by Dunn and coworkers at Calspan, e.g. Dunn (1990), Dunn *et al.* (1984). The reasons are that their work includes high time resolution heat flux measurements obtained using a transient thin film heat flux guage and that theie experiments were very close to the real world conditions.

Of greater interest to this work is their review of cascade experiments, of which the more important is the work of Langston *et al.* (1977) and Graziani *et al.* (1980), which provides a database suited for code validation. A more recent database covering a range of Reynolds numbers was compiled by Boyle & Russell (1990). Simoneau & Simon (1993) also state that the role of the detailed but less realistic cascade experiments is to validate codes and physical models. They also included a complete list of cascade experiments conducted before 1993.

In the study by Boyle & Russell (1990) local Stanton numbers are determined for Reynolds numbers based on inlet velocity and axial chord between 73,000 and 495,000 using a uniform heat flux foil and the liquid crystal technique for temperature measurements. Among their conclusions are that the Stanton number patterns are almost independent of both inlet Reynolds number and, which is more surprising, changes in the inlet boundary thickness and that the secondary flow is stronger for the low Reynolds number cases.

Giel *et al.* (1998) measured endwall heat transfer in a rotor cascade using the same method as Boyle & Russell (1990). Measurements are obtained for different Mach and Reynolds numbers with and without turbulence grid. Eight differ-

ent flow conditions were investigated. The endwall heat transfer data presented here, along with the aerodynamic data presented by Giel *et al.* (1996), comprise a complete set of data suitable for CFD code and model validation. Electronic tabulations of all data presented in this paper are available upon request. The same research group also measured the blade heat transfer of the same geometry. The results are given in Giel *et al.* (1999). Kalitzin (1999) computed the heat transfer for this experiment using the $v^2 - f$ and Spalart-Allmaras one-equation turbulence models. It was found that the predictions of the Stanton number show most of the features observed in the experiments but fail to quantitatively predict the heat transfer to the endwall. Similar observations have been made by the turbine cooling group at Siemens, Finspång (Rubensd¨orffer, private communication).

Another experimental/numerical contribution is the work by Jones and coworkers at the University of Oxford. Their annular cascade facility enables short-duration steady flow to be generated at engine-like conditions for up to one second. Spencer & Jones (1996) found that the secondary flow field had a greater influence on the casing endwall heat transfer than the hub endwall heat transfer. This was explained by the fact that the hub vortex had lifted from the endwall closer to the leading edge than the casing endwall vortex. Harvey *et al.* (1999) found, quite in contradiction to other studies, that the heat transfer rate is strongly influenced by the Reynolds number, an effect that was reproduced in calculations. They also found that the main difference between measurements and calculations is that the secondary flow effects on the endwall are underestimated.

In the late 1990s a series of experimental and numerical studies by Thole and coworkes was conducted at the Virginia Polytechnic Institute and State University. They investigated the influence of the freestream turbulence level and inlet conditions on the flow field and heat transfer in a large scale stator vane passage at two Reynolds numbers. One finding was that the vane heat transfer is largely determined by the level of freestream turbulence, showing augmentations of 80% on the pressure side, whereas the heat transfer to the endwall depende to a greater extent on the intensity of the secondary flow field. Further, in Hermanson & Thole (2000*a*) and Hermanson & Thole (2000*b*), the influence of inlet conditions and Mach number effects on the secondary flow is illustrated on the basis of numerical investigations. As detailed measurements of both flow field and heat transfer were available this set of experiment was chosen as test case for the numerical study in this project and will be described in Section 1.4.4.

For a more detailed review of gas turbine endwall research, including both numerical and experimental investigations, see Rubensd¨orffer (2002).

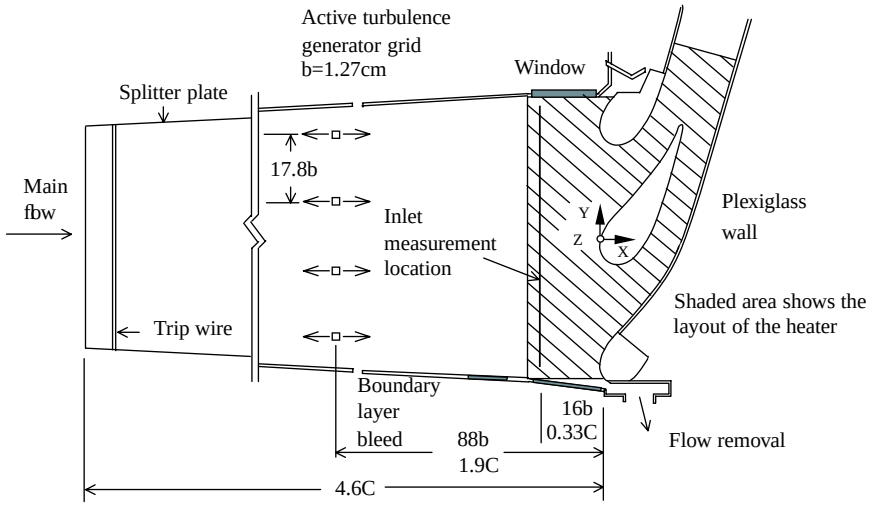

Figure 1.8: A schematic of the experimental stator vane test section (Radomsky, 2000).

1.4.4 Experimental Test Case for Validation

The experiment chosen for validating the computations carried out in the work is a series of measurements from the Virginia Polytechnic Institute and State University, USA, led by Professor Thole. They provide a detailed set of both flow field and heat transfer measurements including documented inlet profiles, a combination rarely found in the literature. This group has conducted several experiments at various inlet turbulence intensities and Reynolds numbers on a scaled-up stator vane at low Mach numbers. A summary of their most important findings is given in Thole *et al.* (2002).

In the part of the present thesis in which secondary endwall flows are considered, only one of the documented experiments, given in Kang & Thole (2000), was numerically investigated. This case is a low turbulence intensity case ($\mathrm{Tu} = 0.6\%$) with an exit Reynolds number of $\mathrm{Re}_{ex} = 1,200,000$. A schematic of the experimental set-up is given in Figure 1.8. For a detailed description of the rig design see Kang *et al.* (1999).

1.5 Transition to Turbulence

Turbulence modelling has for several decades been subject to intense research and has reached some level of maturity. Today turbulence models exist that are able to provide accurate predictions of turbulence effects on the mean flow characteristics, given that the mean flow itself is not too complicated. In flows where more complex flow features are present, turbulence models still lack in reliability and require a more careful (critical) analysis of computed data, at least until new, even more powerful methods are developed.

There is however one phenomenon that can cause the most advanced turbulence model to fail in flows that are seemingly the most straightforward to compute, e.g. the flow over a flat plate. This phenomenon is the transition of a laminar flow into a turbulent state and has been studied extensively since Osbourne Reynolds, in 1883, was able to relate the parameter $\rho V d/\mu$ to the change in flow behavior as the flow makes a transition to turbulence. The reason for the great interest in transition is not only that it plays an important role in many engineering applications but also that it raises a more fundamental question about the nature of flow physics and is an example of the problem of determinism and chaos. It was only recently, with the aid of Direct Numerical Simulations, that all details of the mechanisms behind transition began to become clearer.

A particular field in which there has recently been increased interest in transition physics and its modelling is turbomachinery design. In gas turbines, for example, transitional phenomena are crucialto the design of the compressor and the turbines. In the former, about half the loss of stage efficiency at the design point owes to skin friction, which is several times larger in a turbulent boundary layer than in its laminar counterpart. When the compressor is run at off design conditions, however, losses commonly rise rather dramatically as an effect of flow separation. The extent of the separated regions is largely influenced by the state of the flow in the separated shear layer. If the separation bubble–which is usually laminar at the point of separation–transitions, it will likely reattach to the blade surface and the loss in efficiency will be limited. Under some circumstances, the transitional process is slow and the flow reattachment point may move far downstream on the suction surface and, here, the large separated region causes severe losses in stage efficiency. It thus becomes evident that there is a trade-off between the increase in skin friction losses at design and the risk of massive separation at off design. The compressor designer must also be aware of the complex interplay between separation and transition at off design conditions. These arguments also apply to the turbine of the gas turbine engine. Here the situation is further complicated by the high temperature environment, and boundary layer transition (to turbulence) dramatically increases the heat load on the turbine airfoils.

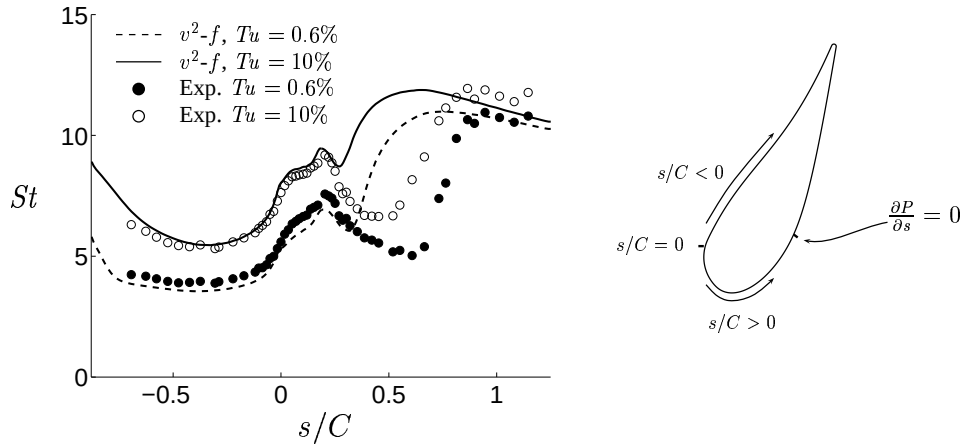

Figure 1.9: Illustration of the effect of transition on heat transfer characteristics at two different freestream turbulence levels. To the left the Stanton number (non-dimensionalized heat transfer coefficient) is plotted along the surface coordinate, s, defined in the schematic to the right. The solid and dashed lines show results computed with the $v^2 - f$ turbulence model of Durbin (1995*b*). The suction peak is located at approximately $s/C = 0.5$.

An example of the importance of accurate predictions of the transition process to gas turbine heat transfer is shown in Figure 1.9. Here the measured and computed surface heat transfers are plotted along a coordinate, s, defined in the schematic to the right in Figure 1.9, that sweeps around a typical turbine stator vane[4]. It can be seen that, along the pressure side ($s/C < 0$), where transition never occurs, the predictions agree closely with the experimental data. Note especially the accurate response of the computed results to the change in turbulence freestream conditions. The situation is worse on the suction side ($s/C > 0$). Here the measured onset of transition, indicated by the rapid increase in heat transfer rates, is located at about half a chord length from the leading edge ($s/C \approx 0.5$), with the high freestream turbulence case transitioning the earliest. At both freestream conditions the turbulence model predicts the transition onset location far too early. The consequence is that, for approximately one third of the suction side of the stator vane, the computations overpredict the heat load on the vane by about 100%! Thus, if the design of the turbine were based on the computations only, the vane cooling in the pretransitional area would be considerably overdimensioned.

Today, several trends lead to gas turbines operating at reduced Reynolds numbers. One is that the market for small turbines (25-100 kW) is increasing (UAVs

[4]The measurements were performed by Radomsky (2000).

powered by gas turbines, intracity Internet links, military vehicles). Another is the trend towords higher by-pass ratio engines with reduced noise levels. Lower Reynolds numbers lead to boundary layers that are less likely to transition to a turbulent state and, when they do, the process is usually slower and the length of the transitional part of the boundary layers along the blade surfaces increases. Consequently, the need for accurate predictions of transitional boundary layers also increases.

1.6 Objectives of the Present Study

Let us conclude this introductory chapter by defining the main objectives of the work presented in this thesis. The overall aim has been to evaluate a specific type of turbulence modelling, the elliptic relaxation approach suggested by Durbin (1991), in a complex stator vane flow against a suitable set of experimental data, which was to be chosen from the existing literature. As reliable (turbulent) heat flux predictions are of particular interest a requirement for the experimental data set was that local endwall heat transfer data were documented. Such heat transfer data, together with well documented flow field measurements (including turbulence quantities), enable a validation of the chosen turbulence closure's ability to predict turbulence effects on i) the complex three-dimensional mean flow field in a turbine airfoil passage and ii) airfoil passage heat transfer in general and endwall heat transfer in particular.

A second objective of equal importance has been to investigate how important the effects of turbulence really are. For example, are the secondary flow structures significantly influenced by the choice of turbulence closure or are the inviscid terms so great that this choice becomes irrelevant? Another question is whether the increased heat transfer rates resulting from elevated levels of freestream turbulence affect the heat transfer to the endwalls *or* whether a correct representation of the secondary flow features, which was earlier argued to expose the endwalls to hot freestream fluid, is sufficient?

At the startof this work a relatively new turbulence model began to grow in popularity. The model, i.e. the $v^2 - f$ model suggested by Durbin (1991), was claimed to work reasonably well in complex flows involving, for example, flow separation and seemed also to produce promising results in terms of heat transfer predictions. There was thus great interest on the part of the partners involved in this project, who were generally rather disappointed with the reliability of turbulence heat flux modelling, in investigating this model's capabilities in the stator flow introduced above and comparing its performance with that of other turbulence models in everyday use in industry. Thus a more specific task has been to

benchmark the $v^2 - f$ model in gas turbine applications.

Even though the $v^2 - f$ model has showed promising results, it is, in principle, unable to account for turbulence anisotropy. This is a problem, as turbulence heat transfer is known to depend rather strongly on the level of anisotropy. It was therefore decided to investigate the performance of the nonlinear extension to the $v^2 - f$ model suggested by Pettersson-Reif (2000). As the model is still under development it was used only to compute an asymmetric diffuser test case. The aim of this study was to compare the performance of the nonlinear model with the original linear version and investigate whether the added model complexity is worthwhile. Note that the linear model does rather well in this flow, which is known to be extremely sensitive to the turbulence closure, and gets both the large separated region and the friction coefficient (which is related to heat transfer) about right. A second objective was therefore to bring clarity to the reason why the linear $v^2 - f$ model produces such good results in this flow and to identify the underlying mechanisms responsible for the strong sensitivity to turbulence closure.

The final, but perhaps most important, subject dealt with in this thesis, at least if heat transfer is considered, is the problem of determining the state of boundary layers. Consider for example the perfect *turbulence* model that always produces excellent agreement with experimental data in *turbulent* flows. If this model cannot reliably predict a boundary layer transition from laminar to turbulent (or vice versa) it will not be very useful in *predicting*[5] gas turbine boundary layer flows. Further, the $v^2 - f$ model, as almost every other turbulence model, is known to predict transition too early. Therefore, in an effort to increase the $v^2 - f$ model's reliability as a gas turbine design tool, the final aim of the work here was to identify a measure to improve its performance in transitional flows. As many attempts have been made in the past to improve transition modelling it was decided to begin this modelling effort by making a review of the subject. Thereafter, an approach among the ones found suitable in the literature survey was to be adopted to the $v^2 - f$ model. The aim is then that the resulting turbulence model has the properties of the $v^2 - f$ model in turbulent flows and the ability to predict the most important phenomena in transitional regions.

[5]There is of course always a possibility to prescribe the location of transition by suppressing turbulence in regions where it is known from experience that the boundary layer is likely be laminar. Indeed, this is today a commonly used procedure for dealing with transitional flows.

Chapter 2

Turbulence Modelling

2.1 The Closure Problem

As written in the introduction, it is not yet possible to resolve instantaneous turbulent fluctuations in flows of industrial importance. However, the industry today uses numerical simulations of extremely complex fully turbulent flows as an everyday design tool. How is this possible? The answer is that the turbulence itself is of secondary interest in most applications; only its effect on the mean flow characteristics, such as for example the overall drag of a car, is important. This allows for computations where the turbulent fluctuations can be accounted for using statistical measures of turbulence.

The mean flow equations are obtained by averaging the Navier-Stokes equation. The resulting equations, the so called Reynolds Averaged Navier-Stokes equations, read

$$\begin{aligned} \left[\frac{\partial U_i}{\partial t} + U_j \frac{\partial U_i}{\partial x_j}\right] &= -\frac{1}{\rho}\frac{\partial P}{\partial x_i} + \nu \frac{\partial^2 U_i}{\partial x_j^2} - \frac{\partial}{\partial x_j}\left\langle u_i u_j \right\rangle \\ \frac{\partial U_j}{\partial x_j} &= 0 \end{aligned} \tag{2.1}$$

During this procedure all the effects the turbulent fluid motions have on the *averaged* flow field are averaged and represented by the additional term $\langle u_i u_j \rangle$, termed the Reynolds stress[1].

In the process of averaging we got around the problem of resolving the tiny scales of turbulent motions, which substantially reduces the cost of computing turbulent flows. The great reduction in complexity was not free, however, as

[1] It should be emphasized here that no modelling has yet been done and that Eqn 2.1 are exact.

it generated the *unknown* Reynolds stress term. This term, which is actually a symmetric tensor with no less than six unknown components, must somehow be related to other *known* variables in order to obtain a closed system of equations. This modelling requirement is usually referred to as the turbulence closure problem and some of the suggested closures, in particular the so called eddy-viscosity based closures, will be discussed in the following section.

2.2 Turbulence Closures

The concept of eddy-viscosity modelling is the turbulence modelling approach adopted in this study. Before going into its details, however, two alternative methods to model turbulence will be very briefly discussed for completeness. These are Large-Eddy Simulations (LES) and Second Moment Closures (SMC) of which the former usually has a clear coupling to eddy-viscosity modelling.

2.2.1 Large-Eddy Simulation

Consider again the discussion given in the introduction on mixing due to turbulence. There it was argued that the mixing property of turbulent flows is superior to that of laminar flows owing to the presence of motions on a much larger scale than the scale of the molecular motions. The idea behind LES is not that different. The main concept is that most of the turbulent transport characteristics are given by the larger turbulent structures of a flow. The evolution of these 'large' structures is computed using dynamic equations that are almost identical to the Navier-Stokes equations, i.e. they are described with only a minimal amount of turbulence modelling. The difference between this approach and DNS is that the smaller turbulence scales are not resolved and thus require modelling. The eddy-viscosity modelling approach is often adopted for this purpose. As the larger structures in many fluid flows are indeed the ones that chiefly affect the overall flow picture, the modelling of the smaller scales is only of secondary importance. LES may thus be considered an alternative to DNS in which the computational facilities set the bound on the smallest affordable resolved flow structures.

Unfortunately, the dynamic behavior of some flows cannot be characterized by 'large' scale motions alone. The most important examples are flows in which the boundary layer development plays a significant role, which includes all applications in which predictions of heat transfer are important. The problem with boundary layers is that the important scales are not significantly larger than the smallest scales of the flow. Thus, for an LES approach to work properly in a

boundary layer, i.e. to fulfill the requirement of resolving its dynamically important scales, the resolution needs to approach that of a DNS.

A second problem with LES as a numerical tool is its inherent dependence on mesh resolution. Usually, the size of the smallest scales resolved is coupled to the resolution of the numerical grid, i.e. the finer the grid the finer the resolution will be and, thus, grid dependence becomes an issue. In theory this is not a problem. The mesh size can simply be decoupled from the size of the smallest resolved scales and the same flow can be computed on a finer grid. The problem is that there is a tempting alternative: that is, to use the additional grid points to reduce the need for modelling, i.e. to approach DNS.

2.2.2 Second Moment Closures

Second moment closures constitute the most advanced statistical single point[2] turbulence closure approach. The modelling basis is the derivation of transport equations for the six individual components of the Reynolds stress tensor by taking the 'second moment' of the RANS equations (Eqn 2.1). The procedure involves additional averaging, which results in a large number of additional unknown terms that require modelling. The conditions for this approach to be more successful than directly relating the Reynolds stresses to mean flow quantities are that the new unknowns are either easy to model or are of subordinate dynamic importance and that the explicit accessibility of the Reynolds stress components significantly facilitates the modelling of turbulence at a reasonable additional computational expense.

The strength of this approach is that the Reynolds stresses no longer have to be related to *local* flow quantities but are governed by their own transport equations, which allows for nonlocal, or 'history', effects. The drawbacks are i) the large number of unknown source terms in these transport equations, ii) the fact that seven transport equations must be solved for the closure of the Reynolds stresses (six equations for the stresses and one to determine a turbulence length scale, usually an equation for the rate of dissipation), iii) that the resulting source terms in the mean momentum equations become large, which has a destabilizing effect on the numerical solution procedure and iv) that the near wall treatment (with implications for heat transfer predictions) is often problematic.

[2]The term 'single point' refers to the closure of unknown terms using only *local* mean fbw or turbulence quantities.

2.2.3 The Eddy-Viscosity Concept

The impact of both large-eddy simulations and second moment closures in industry is relatively limited. The reasons are likely that LES is still regarded as being too expensive for everyday industrial use and that SMCs are a bit unreliable in terms of numerical stability. Another reason might be a reluctance to abandon well established procedures, with deficiences the experienced CFD is well aware of, for new, more complex methods with a different set of potential pitfalls. Therefore, the absolutely most commonly used turbulence closures are those based on the eddy-viscosity concept[3]. The term is somewhat confusing, however, as it infers that the nature of modelled Reynolds stress effects should be similar to the nature of molecular motion, i.e. that Reynolds stress effects are of a diffusive character. This is not at all the case, as the Reynolds stresses stem from the average of the nonlinear *convective* terms in the Navier-Stokes equations.

In a turbulent flow we know from the exact transport equations for the Reynolds stresses, $\langle u_i u_j \rangle$, that the *generation* of Reynolds stresses is proportional to the mean rate of strain. If we assume that the turbulence responds rather quickly to changes in the mean flow we would expect the Reynolds stresses themselves to be related to the mean rate of strain. This means that large Reynolds stresses will generally be found in areas of high strain, which most likely makes it easier to find an accurate empirical formula for the ratio of a Reynolds stress to the mean rate of strain than a model of the Reynolds stress itself. The most general way to linearly relate the Reynolds stresses to the mean rate of strain using this stress/strain rate ratio concept would be

$$-\langle u_i u_j \rangle = \nu_{t,ijlm} \left(\frac{\partial U_l}{\partial x_m} + \frac{\partial U_m}{\partial x_l} \right) - \frac{2}{3} k \delta_{ij} \tag{2.2}$$

where $\nu_{t,ijlm}$ is the eddy-viscosity. This fourth order tensor requires modelling for the RANS equation to be closed. Using certain properties of this tensor the number of unknowns can be reduced to the order of 50 (Johansson, 2002), which is still too high to be of any practical use. Hence, the most commonly used assumption is to treat the eddy-viscosity as a scalar quantity (for further discussion on this subject see Bradshaw (1996)). Based on dimensional reasoning the eddy-viscosity can be written as the square of a turbulence velocity scale, $\mathcal{V}$, muliplied with a turbulence time scale, $\mathcal{T}$,

$$\nu_t = C_\mu \mathcal{V}^2 \mathcal{T} \tag{2.3}$$

[3]The term eddy-viscosity originates from the model being a direct analogy to the modelling of the viscous stress tensor.

C_μ is usually supposed to be a universal constant, and the Reynolds stresses can now be calculated using

$$-\langle u_i u_j \rangle = -2\nu_t S_{ij} + \frac{2}{3} k \delta_{ij} \tag{2.4}$$

Recall that the eddy-viscosity contains information from both the mean velocity and the turbulence field (cf. Eqn 2.2). Here we have assumed that we can obtain the eddy-viscosity using two local turbulent scales (Eqn 2.3) that only have implicit connections to the mean flow, whereas the stress and the strain rate in Eqn 2.2 are different types of quantities (Bradshaw, 1996). Nevertheless, we have now replaced the unknown Reynolds stresses with the scalar eddy-viscosity multiplied by the rate of strain tensor. The scalar eddy-viscosity is in turn modelled by introducing *two* new unknown quantities: a turbulence velocity and a turbulence time scale. Both these scales require modelling, and the following sections give some examples of how they can be estimated from (known) mean flow variables using transport equations for turbulence quantities.

2.2.4 The Standard $k - \varepsilon$ Model

The number of $k - \varepsilon$ turbulence models that can be found in literature is vast. The first one suggested is the high Reynolds number model of Jones & Launder (1972), usually referred to as the 'standard' $k - \varepsilon$ model. This model has been followed by many modified versions that often outperform the original. The main reason why it is introduced here is that it is a cornerstone in the more advanced $v^2 - f$ model described in Section 2.2.5, which is used extensively in this work.

The $k - \varepsilon$ turbulence model is based on the exact transport equations for the turbulent kinetic energy, k, and its dissipation rate, ε (the derivation of the k equation can be found in Wilcox (1993), which also outlines the derivation of the ε equation). $k^{1/2}$ directly gives the velocity scale needed to close Eqn 2.3. To get the time scale we can use the same velocity scale together with a length scale, i.e. $\mathcal{T} = L/k^{1/2}$. This length scale is given in $k - \varepsilon$ models by $L = k^{3/2}/\varepsilon$; hence the ε equation is sometimes referred to as a length scale determining equation[4].

Without going into any modelling details the modelled k and ε equations read

$$\frac{\partial k}{\partial t} + u_j \frac{\partial k}{\partial x_j} = \frac{\partial}{\partial x_j}\left(\left(\nu + \frac{\nu_t}{\sigma_k}\right)\frac{\partial k}{\partial x_j}\right) + P_k - \varepsilon \tag{2.5}$$

$$\frac{\partial \varepsilon}{\partial t} + u_j \frac{\partial \varepsilon}{\partial x_j} = \frac{\partial}{\partial x_j}\left(\left(\nu + \frac{\nu_t}{\sigma_\varepsilon}\right)\frac{\partial \varepsilon}{\partial x_j}\right) + \frac{C_{\varepsilon 1} P_k - C_{\varepsilon 2}\varepsilon}{\mathcal{T}} \tag{2.6}$$

[4]Several turbulence researchers have suggested transport equations for different combinations of $k^m L^n$ in order to determine the turbulent length scale (once the new quantity is known, L can be resolved), cf. Wilcox (1993).

where $\mathcal{T} = k/\varepsilon$. $\mathcal{T}$ goes to zero near walls causing a singularity in the ε equation. To avoid numerical problems owing to this singularity Durbin (1991) suggested a lower bound on the time scale using the Kolmogorov variables, $\mathcal{T} \geq 6\sqrt{\nu/\varepsilon}$.

The ε wall boundary condition, which will be derived in Section 2.4, used in the $v^2 - f$ model reads

$$\varepsilon \rightarrow 2\nu \frac{k}{y^2} \qquad \text{as } \; y \rightarrow 0 \tag{2.7}$$

The following notation will frequently be used hereafter:

$$P_k = 2\nu_t S^2, \quad S^2 = S_{ij} S_{ij}, \quad S_{ij} = \frac{1}{2}\left(\frac{\partial U_i}{\partial x_j} + \frac{\partial U_j}{\partial x_i}\right) \tag{2.8}$$

where P_k is the production of turbulent kinetic energy, i.e. a measure of the rate of conversion of mean flow kinetic energy into turbulent kinetic energy. In reality this process can also take place in the reverse direction ('negative' production), but the assumptions made in deriving the scalar eddy-viscosity (with constant C_μ) only allow for energy transport in one direction. Finally, the standard $k-\varepsilon$ model coefficients are

$$C_\mu = 0.09, \quad C_{\varepsilon 1} = 1.44, \quad C_{\varepsilon 2} = 1.92, \quad \sigma_k = 1.0, \quad \sigma_\varepsilon = 1.3 \tag{2.9}$$

2.2.5 The $v^2 - f$ Model

The different versions of the $v^2 - f$ turbulence models of today are all based on the standard $k-\varepsilon$ model. That is, the model equations are solved without so called low Reynolds number damping functions. k and ε are used to form the turbulent time scale, $\mathcal{T}$ (cf. Eqn 2.3). The $v^2 - f$ model differs from the family of two-equation models in that here an additional velocity scale, v^2, is provided and used as the turbulent velocity scale, $\mathcal{V} = (v^2)^{1/2}$, i.e. not the usual $k^{1/2}$. The new scalar, v^2, which can be regarded as the energy of fluctuations normal to streamlines, is obtained by solving an additional transport equation.

In all, the $v^2 - f$ model requires solving the standard $k - \varepsilon$ equations together with the additional equation for v^2 that in turn has a source term governed by a fourth differential equation. This of course increases the computational requirements by some 30% as compared with two-equation models, as we must find solutions to, in total, nine instead of seven partial differential equations. Still, it is cheaper than second moment closures, which require solving twelve PDEs.

The increased computational cost can be justified by considering a fully developed turbulent wall boundary layer. By examining the mean flow momentum

equation we see that the only Reynolds stress component felt by the mean flow is the shear stress $\langle uv \rangle$. Hence, in order to predict the mean flow, we must have a sufficiently good model for this stress component. From the exact transport equation for $\langle uv \rangle$, its production rate, P_{uv}, is given by

$$P_{uv} = - \left\langle v^2 \right\rangle \frac{dU}{dy} \tag{2.10}$$

As no other term is taken into account in eddy-viscosity modelling we assume that the shear stress itself divided by some typical turbulent time scale will be proportional to P_{uv}, i.e.

$$\frac{\langle uv \rangle}{\mathcal{T}} \sim P_{uv} \tag{2.11}$$

Hence,

$$\langle uv \rangle \sim \mathcal{T} P_{uv} = - \left\langle v^2 \right\rangle \mathcal{T} \frac{dU}{dy} \tag{2.12}$$

Using the scalar eddy-viscosity approach outlined in Section 2.2 the modelled shear stress component is calculated according to

$$- \langle uv \rangle = C_\mu \mathcal{V}^2 \mathcal{T} \frac{dU}{dy} \tag{2.13}$$

which is exactly the expression in Eqn 2.12 if the constant of proportionality is C_μ and the velocity scale is chosen to be $\langle v^2 \rangle^{(1/2)}$. It is thus clear that the proper velocity scale upon which to base the eddy-viscosity model in order to correctly model the shear stress in a fully developed channel flow should be $\langle v^2 \rangle^{(1/2)}$. That the fluctuating velocity component normal to shear layers is important to the generation of turbulence is not a new finding. For example, Phillips (1969) investigated an eddy-viscosity based generation mechanism of Reynolds stress in an analytical analysis of homogeneous shear flow. He illustrated the nonlocality of the Reynolds stresses as well as that the eddy-viscosity can in a sense be considered a local property (in the flow studied) and that the eddy-viscosity is proportional to the kinetic energy of the vertical fluctuations and the convected time scale of these fluctuations.

As mentioned, the standard estimate for the velocity scale is the turbulence kinetic energy, $k^{(1/2)}$. Section 2.4 will show that, in the vicinity of solid walls, $k \sim y^2$ and $\langle v^2 \rangle \sim y^4$, i.e. the damping of the velocity scale, v^2, is much stronger than the damping of k due to the kinematic blocking of the wall. Thus models with velocity scales $k^{(1/2)}$ are generally expected to require additional near wall damping to be able to reproduce the dependence of $\langle uv \rangle$ on the distance to the wall. To

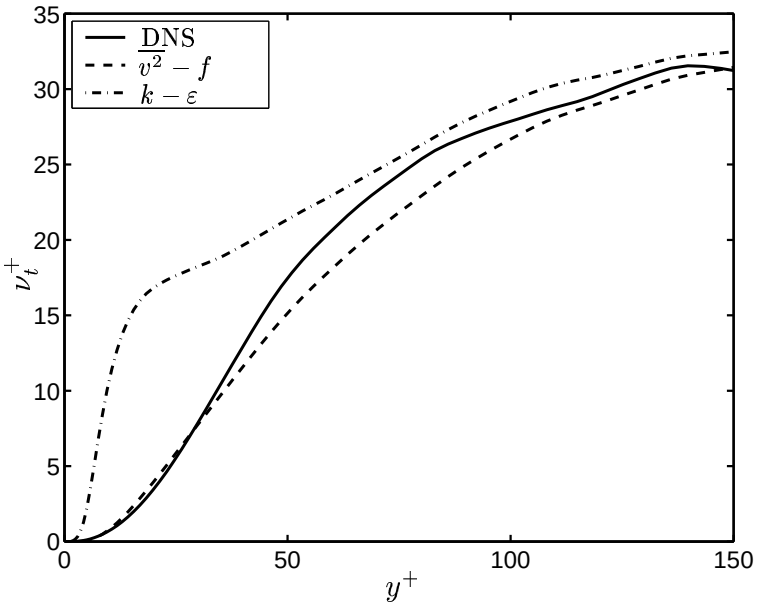

Figure 2.1: Normalized turbulent viscosity for different ν_t closures computed from DNS data

illustrate this further we may scrutinize the different relations by explicitly evaluating them using DNS data. Figure 2.1 plots the normalized eddy-viscosity for the plane channel DNS data of (Moser *et al.*, 1999). The DNS eddy-viscosity was computed according to its definition, $\nu_t = -\langle uv \rangle / \frac{dU}{dy}$, while the $k-\varepsilon$ and $v^2 - f$ eddy-viscosities were obtained from $\nu_t = C_\mu k^2/\varepsilon$ and $\nu_t = C_\mu \langle v^2 \rangle k/\varepsilon$, respectively. As pointed out by Durbin (1991), the standard $k-\varepsilon$ model fails to reproduce the true eddy-viscosity simply because the y dependence of k^2/ε is wrong (in low Reynolds number $k-\varepsilon$ models this is fixed by introducing a damping function defined as the ratio between $C_\mu k^2/\varepsilon$ and ν_t). We also see in Figure 2.1 that if we somehow have the $\overline{v^2}$ distribution we can get a very good estimate of ν_t, especially in the important near wall region, without using damping functions.

The ideas described in short above led to a modelled v^2 equation, suggested by Durbin (1991, 1993, 1995*b*), of the following form (additional modelling arguments are given in Sveningsson (2003))

$$\frac{\partial v^2}{\partial t} + u_j \frac{\partial v^2}{\partial x_j} = \frac{\partial}{\partial x_j}\left(\left(\nu + \frac{\nu_t}{\sigma_k}\right)\frac{\partial v^2}{\partial x_j}\right) + kf - \frac{v^2}{k}\varepsilon \qquad (2.14)$$

At first sight there is no evidence of how this equation can have any of the near wall properties that we wanted it to have. The key is the flow variable, f, which is related to the pressure-strain redistribution term and is governed by a modified

Helmholtz equation of an elliptic nature

$$L^2 \frac{\partial^2 f}{\partial x_j^2} - f = \underbrace{\frac{C_1}{T}\left(\frac{v^2}{k} - \frac{2}{3}\right)}_{\phi_{22,S}} \underbrace{-C_2 \frac{P_k}{k}}_{\phi_{22,R}} - \frac{1}{T}\left(\frac{v^2}{k} - \frac{2}{3}\right) \tag{2.15}$$

As kf is the modelled effect of the pressure-strain term, ϕ_{22}, in the v^2 equation, f can be interpreted as ϕ_{22}/k. Launder *et al.* (1975) disusses different models for ϕ_{ij}. Terms $\phi_{22,S}$ and $\phi_{22,R}$ in Eqn 2.15 are the so called slow and rapid pressure-strain terms discussed in this paper. The last term on the right hand side was added to ensure correct farfield behavior, whereas the ellipticity is introduced via the left hand side differential operator.

Modelling the pressure-strain term in the v^2 equation with kf is argued to account in part for the nonlocal kinematic blocking of the wall normal stress component. This important feature of wall bounded turbulent flows is usually not captured using single point closure models without the use of *ad hoc* damping functions. Note that the pressure in a fluid flow is of an elliptic nature, and therefore the correlation of fluctuating pressure and fluctuating velocity gradient (the pressure-strain) is therefore also elliptic. A thorough discussion of this subject is given in Manceau *et al.* (2001), who investigated how pressure-strain is affected by inhomogeneity and anisotropy.

2.2.6 Nonlinear Eddy-Viscosity Models

Section 2.2.3 discussed the most general way to *linearly* relate the Reynolds stress tensor to the mean rate of strain and how this relation had to be simplified to result in a practically ameanable closure model. It is however possible to extend linear models by introducing higher order terms, as suggested by Pope (1975). He showed that the most general way to relate the Reynolds stress tensor to the mean strain rate and rotation rate tensors could be expressed as a finite sum of linearly independent tensors (formed from the strain and rotation rate tensors) that each are multiplied with coefficients that are functions of a finite number of tensor invariants.

In the framework of eddy-viscosity modelling, the most general constitutive equations for two-dimensional mean flows that relate the *a priori* unknown components of the Reynolds stress tensor $\langle u_i u_j \rangle$ to the mean flow field are given in the form (cf. e.g. Pope, 1975):

$$a_{ij} = -C^*_{\mu 1} S_{ij} - C^*_{\mu 2}\left(S_{ik}\Omega_{kj} + S_{jk}\Omega_{ki}\right) + C^*_{\mu 3}\left(S_{ik}S_{kj} - \frac{1}{3}S^2\delta_{ij}\right) \tag{2.16}$$

where $a_{ij} = \langle u_i u_j \rangle / k - 2/3\delta_{ij}$ is the turbulence anisotropy tensor and S_{ij} and Ω_{ij} are the components of the mean rate of strain and local mean vorticity tensors, respectively. Coefficients $C^*_{\mu i}$ are related to known turbulence quantities and the tensor invariants mentioned above ($S_{ij}S_{ji}$ and $\Omega_{ij}\Omega_{ji}$ in two dimensions).

Under the condition that the transport of the Reynolds stresses can be accurately modelled using

$$\text{transport of } \langle u_i u_j \rangle \approx \frac{\langle u_i u_j \rangle}{k} (P_k - \varepsilon) \tag{2.17}$$

Pope (1975) showed that a nonlinear eddy-viscosity approach would predict the same Reynolds stresses as full second moment closures, which is a great improvement as compared with linear eddy-viscosity models. Note that no additional transport equation has to be solved and the computational cost is therefore approximately of the same order as that of linear eddy-viscosity models. Paper III illustrates the potential of this type of modelling.

2.3 Turbulence Diffusion Models

2.3.1 The Eddy-Diffusivity Concept

The exact transport equations for all turbulence quantities involve divergence terms that must be modelled. As an example, consider the turbulence kinetic energy equation (turbulence) divergence terms, D_k,

$$D_k = \frac{\partial}{\partial x_j} \left(-\frac{1}{\rho} \langle p u_i \rangle \delta_{ij} - \left\langle \frac{1}{2} u_i u_i u_j \right\rangle \right) \tag{2.18}$$

In all turbulence models based on eddy-viscosity these divergence terms are modelled in the same way that the diffusion caused by molecular motions is modelled, that is, by introducing a new viscosity, the eddy-viscosity, and arguing that the flux of the transported quantity (here k) due to the unclosed terms in Eqn 2.18 will always be directed from regions of high levels of k towards regions of lower levels of k. The rate at which this transport proceeds is given by the eddy-viscosity divided by a quantity specific Prandtl number. Thus, the model adopted for D_k is

$$D_k \approx \frac{\partial}{\partial x_j} \left(\frac{\nu_t}{\sigma_k} \frac{\partial k}{\partial x_j} \right) \tag{2.19}$$

This approximation is very crude. The whole idea of modelling transport by turbulence motion, which is always due to convective transport, with a diffusivity

based concept is inauspicious. However, considering the persistence of this closure concept, more physically realistic models based on the limited flow information provided by eddy-viscosity closures are not likely to appear. It is therefore fortunate that the turbulence equations when applied to many flows of engineering interest are dominated by their source terms and that here diffusion plays only a subordinate role.

Finally, it is worth mentioning that the Prandtl number that varies the most from one numerical study to another is that used to model turbulent transport of heat. It usually lies in the range of 0.6-0.9; in this study a value of 0.89 has been adopted.

2.3.2 The Generalized Gradient Diffusion Hypothesis

In cases where an accurate representation of the individual Reynolds stresses is available (i.e. more accurate than (linear) eddy-viscosity models offer), it is often beneficial to use this anisotropy information to improve the turbulent transport model. The by far most commonly used 'higher order' model is the Generalized Gradient Diffusion Hypothesis (GGDH) of Daly & Harlow (1970),

$$D_\phi = \frac{\partial}{\partial x_m}\left(C_\phi \overline{u_m u_n} T \frac{\partial \phi}{\partial x_n}\right). \tag{2.20}$$

where ϕ represents any flow variable, T is a turbulence time scale, usually k/ε, and C_ϕ is a model constant. This model was investigated in Paper III, where a fairly accurate representation of $\langle u_i u_j \rangle$ was available from the nonlinear eddy-viscosity model used in that study.

2.4 Wall Boundary Conditions for some Turbulent Quantities

In this section the wall boundary conditions for the modelled dissipation rate, ε, and the relaxation parameter, f, are derived. For a review of near wall turbulence modelling including analysis of near wall behavior of turbulent quantities the reader is referred to Patel *et al.* (1985).

The ε wall boundary condition

The boundary value of turbulent kinetic energy on a solid wall is zero due to the no-slip concept. In order to obtain the boundary condition for the dissipation rate

of turbulent kinetic energy, the fluctuating velocities are expanded according to

$$\begin{aligned} u &= a_0 + a_1 y + a_2 y^2 \ldots \\ v &= b_0 + b_1 y + b_2 y^2 \ldots \\ w &= c_0 + c_1 y + c_2 y^2 \ldots \end{aligned} \tag{2.21}$$

The coefficients can be functions of anything but y, and they are zero if averaged. The no-slip condition gives $a_0 = b_0 = c_0 = 0$. Continuity and the fact that $(\partial u/\partial x)_{y=0} = (\partial w/\partial z)_{y=0} = 0$ (no-slip) gives $(\partial v/\partial y)_{y=0} = 0$. Therefore b_1 too must be equal to zero and the behavior of the wall normal and tangential Reynolds stresses is found by squaring and averaging the expressions for the fluctuating velocities. The sum of these three stresses gives twice the turbulent kinetic energy.

$$\begin{aligned} \left\langle u^2 \right\rangle &= \left\langle a_1^2 \right\rangle y^2 + \mathcal{O}(y^3) \\ \left\langle v^2 \right\rangle &= \left\langle b_2^2 \right\rangle y^4 + \mathcal{O}(y^5) \\ \left\langle w^2 \right\rangle &= \left\langle c_1^2 \right\rangle y^2 + \mathcal{O}(y^3) \\ k &= \frac{1}{2}\left(\left\langle a_1^2 \right\rangle + \left\langle c_1^2 \right\rangle\right) y^2 + \mathcal{O}(y^3) \end{aligned} \tag{2.22}$$

The modelled (homogeneous) dissipation rate is defined as:

$$\varepsilon \equiv \nu \left\langle \frac{\partial u_j}{\partial x_i} \frac{\partial u_j}{\partial x_i} \right\rangle \tag{2.23}$$

We will now show that we can express the near wall dissipation rate in terms of the kinetic energy itself and use this relation as a boundary condition for ε.

In the vicinity of walls, all $\partial/\partial x$ and $\partial/\partial z$ terms are negligible compared to the $\partial/\partial y$ terms and we can use the Taylor expansions for the fluctuating velocities in Eqn 2.21 to estimate the dissipation rate near walls. We get

$$\begin{aligned} \varepsilon &\approx \nu \left(\left\langle \left(\frac{\partial u}{\partial y} \right)^2 \right\rangle + \left\langle \left(\frac{\partial w}{\partial y} \right)^2 \right\rangle \right) \\ &= \nu \left(\left\langle a_1^2 \right\rangle + \left\langle c_1^2 \right\rangle \right) + \mathcal{O}(y) \end{aligned} \tag{2.24}$$

The same quantity as for the kinetic energy (Eqn 2.22), $\langle a_1^2 \rangle + \langle c_1^2 \rangle$, appears, which allows us to express the near wall behavior of ε in terms of k according to

$$\varepsilon \to 2\nu \frac{k}{y^2} \quad \text{as} \quad y \to 0 \tag{2.25}$$

Hence, the two wall boundary conditions used are $k = 0$ and that ε/ν and $2k/y^2$ must have the same limit (i.e. $\langle a_1^2 \rangle + \langle c_1^2 \rangle$) as walls are approached. The correct

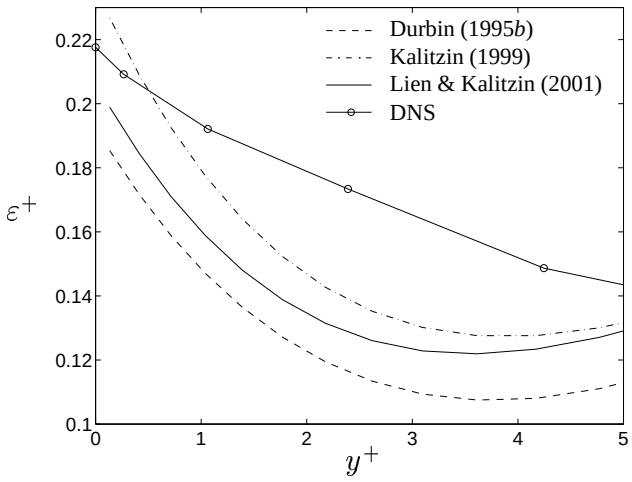

Figure 2.2: Near-wall dissipation rate for DNS data and two versions of the $\overline{v^2}-f$ model. The models of Kalitzin (1999) and Lien & Kalitzin (2001) differ only in model constants and have a $f = 0$ wall boundary condition. The model of Durbin (1995*b*) uses the more unstable f boundary condition given in Eqn 2.29.

lilmit is enforced by forcing ε to take this value at the first interior computational node.

Note that in this derivation we have assumed that the higher order terms in the Taylor expansion of ε can be neglected compared to the zero order term ε_{wall}, i.e. that ε really is constant for y^+ values lower than the y^+ value of the first node, which is typically in the order of 1. In Figure 2.2 the ε profiles from DNS data and two $\overline{v^2}-f$ models (the model of Durbin (1995*b*) and the model of Lien & Kalitzin (2001) with two different sets of model constants) are plotted for $0 < y^+ < 5$. Clearly, the assumption of ε being constant at $y^+ \approx 1$ can be questioned. Therefore the ε boundary condition is always specified at the first interior node. If ε really was approaching a constant value at the first interior node, the natural boundary condition that should be specified would be $\partial\varepsilon/\partial y = 0$.

The f Boundary Condition

The no-slip boundary condition for the velocity scalar, v^2, is $v^2 = 0$. To get a wall boundary condition for f we must study the v^2 equation, which at a small distance from walls reads

$$\nu\frac{\partial^2 v^2}{\partial y^2} - v^2\frac{\varepsilon}{k} + kf = 0 \tag{2.26}$$

In this equation k is replaced using Eqn 2.25 (assuming it is valid) and the equation can be written as

$$\frac{\partial^2 v^2}{\partial y^2} - 2\frac{v^2}{y^2} + \frac{\varepsilon f}{2\nu^2} y^2 = 0 \tag{2.27}$$

Close to walls (very close) f and ε are constant with respect to y and the ordinary differential equation can be solved. The solution is

$$v^2 = Ay^2 + \frac{B}{y} - \varepsilon f \frac{y^4}{20\nu^2} \tag{2.28}$$

and for v^2 to behave as $\mathcal{O}(y^4)$ the integration constants, A and B, must be equal to zero. Hence, the boundary condition for f is

$$f \to -\frac{20\nu^2}{\varepsilon}\frac{v^2}{y^4} \quad \text{as} \quad y \to 0 \tag{2.29}$$

Unfortunately, this boundary condition makes the $v^2 - f$ model numerically unstable. The stability can be improved by solving the v^2 and f equations in a coupled manner (Section 3.4.2 will describe the implementation of a coupled TDMA solver used in this project). Another more popular method to circumvent this problem is to redefine the f variable such that the wall boundary condition for f becomes $f = 0$. The performance of the two different approaches was investigated in a stator vane flow field by Sveningsson (2003), where the exact details of the models are given.

2.5 Realizability

A common deficiency in turbulence models based on eddy-viscosity is that they overpredict the turbulent kinetic energy (TKE) in stagnation point flows. Durbin (1995*a*) suggested the use of a "realizability" constraint, $2k \geq \langle u_i^2 \rangle \geq 0$, in order to limit the growth of TKE in regions where standard eddy-viscosity based expressions for the Reynolds stresses take erroneous values. Durbin expressed this constraint in terms of a limit on the turbulent time scale, $\mathcal{T}$, which greatly improves TKE predictions.

2.5.1 Derivation of the Time Scale Constraint

Most eddy-viscosity based turbulence models use the following expression when calculating the Reynolds stresses appearing in the RANS equations

$$\langle u_i u_j \rangle = -2\nu_t S_{ij} + \frac{2}{3} k \delta_{ij} \tag{2.30}$$

It is well known that this model gives abnormal levels of TKE in stagnation regions. This problem can be dealt with in several ways, of which the Kato & Launder (1993) '$S_{ij}\Omega_{ij}$' (cf. Section 2.5.3) and the Durbin (1995*a*) time scale approaches are the most commonly used.

Durbin showed that the constraint $\langle u^2 \rangle \geq 0$ can be used to derive a bound on the turbulent time scale, $\mathcal{T}$ (e.g. k/ε in k-ε models). This constraint is imposed by finding the eigenvectors of S_{ij}, i.e. rotating the coordinate system so that the strain rate tensor, S_{ij}, becomes diagonal with eigenvalues λ_α, $\alpha = 1, \ldots, 3$. In this worst case coordinate system (our constraint $\langle u^2 \rangle \geq 0$ must be fulfilled in any coordinate system), all strains are normal and Eqn 2.30 can be written as

$$\left\langle u_\alpha^2 \right\rangle = -2\nu_t \lambda_\alpha + \frac{2}{3}k \tag{2.31}$$

Imposing our constraint $\langle u^2 \rangle \geq 0$ gives

$$2\nu_t \lambda_\alpha \leq \frac{2}{3}k \tag{2.32}$$

Solving the characteristic equation for λ_α we have that $|\lambda_\alpha| = \sqrt{S^2/2}$ in two dimensions and that

$$|\lambda_\alpha| \leq \sqrt{2S^2/3} \tag{2.33}$$

in three dimensions. Equations 2.32 and 2.33 may now be used to obtain a lower limit on ν_t

$$\nu_t \leq \frac{k}{3 \max \lambda_\alpha} \tag{2.34}$$

Now insert Eqn 2.3 for ν_t to obtain

$$C_\mu \mathcal{V}^2 \mathcal{T} \leq \frac{k}{3 \max \lambda_\alpha} \tag{2.35}$$

Division by $C_\mu \mathcal{V}^2$ gives the constraint that Durbin uses, i.e.

$$\mathcal{T} \leq \frac{k}{3C_\mu \mathcal{V}^2} \frac{1}{\max \lambda_\alpha} \tag{2.36}$$

For k-ε models this implies

$$\mathcal{T} = \min \left(\frac{k}{\varepsilon}, \frac{1}{3C_\mu} \frac{1}{\max \lambda_\alpha} \right) \tag{2.37}$$

whereas for $\overline{v^2}$-f models

$$\mathcal{T} = \min \left(\max \left(\frac{k}{\varepsilon}, 6\sqrt{\frac{\nu}{\varepsilon}} \right), \frac{k}{3C_\mu v^2} \frac{1}{\max \lambda_\alpha} \right) \tag{2.38}$$

and for k-ω models

$$\mathcal{T} = \min\left(\frac{1}{\omega}, \frac{1}{3\gamma^* \max \lambda_\alpha}\right) \tag{2.39}$$

The above idea originates from investigating the turbulent time scale near stagnation points where it is argued that $\mathcal{T}$ becomes very large. The too high values of $\mathcal{T}$ lead to an underestimation of the modelled production of the dissipation rate in the ε equation. The consequence will be too low an estimate of ε, which explains the high levels of TKE. However, this argument seems to be wrong, which can be seen at a closer look at the source terms in the ε equation that read

$$\frac{C_{\varepsilon 1} 2\nu_t S_{ij} S_{ij} - C_{\varepsilon 2}\varepsilon}{\mathcal{T}} \tag{2.40}$$

or

$$2C_{\varepsilon 1} C_\mu v^2 S_{ij} S_{ij} - \frac{C_{\varepsilon 2}\varepsilon}{\mathcal{T}} \tag{2.41}$$

where Eqn 2.8 and 2.3 have been used to replace the TKE production term, P_k, in the ε equation.

Now it is obvious that the effect that a limitation of the time scale has in the ε equation is not to increase the production of ε but to increase its dissipation. The increase in dissipation of ε will lower the level of ε, i.e. decrease the dissipation rate of TKE, and lead to *higher* levels of TKE. As the time scale bound was introduced in order to decrease the TKE, the effect of limiting $\mathcal{T}$ in the ε equation cannot be the reason why the time scale bound idea works so well.

The reason why the realizability constraint works is the effect of the time scale limitation in the expression for the turbulent viscosity, Eqn 2.3. This relation used in the formula for production of TKE gives

$$P_k = 2C_\mu v^2 \mathcal{T} S_{ij} S_{ij} \tag{2.42}$$

Obviously a decrease in $\mathcal{T}$ will also decrease the production rate of k. Hence, this must be the explanation for the improvement in the predictions of the turbulent kinetic energy levels.

Of even greater practical importance is that the use of the realizable time scale constraint in the f equation has a potential to cause numerical problems (cf. Svensingsson & Davidson, 2004). These numerical problems, which were attributed to the use of the time scale constraint, were in fact the reason why the constraint was analyzed in this project in the first place.

Finally, it should be mentioned that a constant is usually added to the realizability constraint to allow for tuning against experimental data, i.e.

$$\nu_t \leq \frac{C_{lim} k}{3 \max \lambda_\alpha} \tag{2.43}$$

The most commonly used value of C_{lim} is 0.6.

2.5.2 Alternative Applications of the Constraint

It is clear from the above discussion on the working principles of the realizability constraint that it is sufficient to use the constraint in terms of an upper limit of the computed eddy-viscosity, i.e.

$$\nu_t \leq \frac{k}{3\max\lambda_\alpha} = \frac{k}{\sqrt{6}S} \tag{2.44}$$

where the latter equality is valid for three-dimensional computations and is the most frequently used. Note that the limitation in two-dimensional computations is not equally strong ($\nu_t \leq k/\sqrt{4.5}S$).

In the present study it was also found that the numerical stability of the $v^2 - f$ model could sometimes be improved by deriving a constraint on the v^2/k ratio from Eqn 2.44 to be used in the v^2 and f equations. Inserting the definition of ν_t gives

$$\frac{v^2}{k} \leq \frac{1}{\sqrt{6}C_\mu\tau S} \tag{2.45}$$

with

$$\tau = \max\left(\frac{k}{\varepsilon}, 6\sqrt{\frac{\nu}{\varepsilon}}\right) \tag{2.46}$$

Finally, Lien & Kalitzin (2001) suggested a similar bound on the turbulent length scale, L, appearing in the f equation only, according to

$$L = C_L\max\left(\min\left(\frac{k^{3/2}}{\varepsilon}, \frac{k^{3/2}}{\sqrt{6}C_\mu v^2 S}\right), C_\eta\frac{\nu^{3/4}}{\varepsilon^{1/4}}\right) \tag{2.47}$$

Computations of a the flow in a stator vane passage indicate that the level of TKE, once the solution is fully converged, is not very sensitive to how realizability is used in the v^2 and f equations. Worth noting, however, is that the order in which the different limits (the realizability and Kolmogorov limits) are implemented is of importance. It has to be decided which of the limits is the most important and this limit should be executed last in order. Note also that Eqn 2.38 and 2.47 are not consistent in this respect.

2.5.3 Alternatives to the Realizability Constraint

The Kato-Lauder Modification

In linear eddy-viscosity based turbulence models the production of turbulence kinetic energy needs no modelling once the eddy-viscosity closure of the Reynolds

stresses is adopted and the expression for these models may be written as

$$P_k \equiv - \langle u_i u_j \rangle \frac{\partial U_i}{\partial x_j} = 2\nu_t S_{ij} S_{ij} = 2\nu_t S^2 \tag{2.48}$$

In regions of irrotational strain the presence of the modulus of the strain rate tensor often causes problems. Consider for example a nearly isotropic ($\langle u^2 \rangle \approx \langle v^2 \rangle \approx \langle w^2 \rangle$) two-dimensional flow approaching a stagnation point. The exact contributions of the normal Reynolds stress components to the production will be

$$P_k = - \left(\langle u^2 \rangle \frac{\partial U}{\partial x} + \langle v^2 \rangle \frac{\partial V}{\partial y} \right) \tag{2.49}$$

Thus, since $\langle u^2 \rangle \approx \langle v^2 \rangle$ and, from continuity, $\partial U/\partial x = -\partial V/\partial y$, the contributions from these two terms should cancel. The eddy-viscosity expression on the other hand gives

$$P_k = 2\nu_t S_{ij} S_{ij} = \frac{1}{2}\nu_t \left(\left(\frac{\partial U}{\partial x} \right)^2 + \left(\frac{\partial V}{\partial y} \right)^2 \right) \tag{2.50}$$

and the squares of the velocity gradients make them both contribute to a rise in turbulence kinetic energy.

To avoid this problem Kato & Launder (1993) suggested a modification of the expression for P_k according to

$$P_k = 2\nu_t S \Omega \tag{2.51}$$

where

$$\Omega = \sqrt{\Omega_{ij}\Omega_{ij}} \quad \text{and} \quad \Omega_{ij} = \frac{1}{2} \left(\frac{\partial U_i}{\partial x_j} - \frac{\partial U_j}{\partial x_i} \right) \tag{2.52}$$

As the diagonal terms of Ω_{ij} are zero (unless any system rotation is imposed!) this modification improves the prediction of k in stagnation regions, even though it is wrong in principle (it is within the model of $\langle u_i u_j \rangle$ that the error lies). In addition, there are studies that suggest that this modification might worsen production rate predictions in flows with curvature (cf. Craft, 2002).

Neglecting Production by Irrotational Mean Strain Rates

A different way to address the problem of having individual irrotational strain rates producing turbulence kinetic energy when they should approximately cancel is simply to neglect them. This can be done by locally transforming the strain rate

tensor, S_{ij}, to a coordinate system with one basis aligned with the velocity vector. The transormed tensor, S'_{ij}, is then used to evalute the modified production by neglecting the contribution of its normal components.

The transformation matrix, $\mathbf{T}$, tested in this project was computed in the following way:

$$\mathbf{T} = (\mathbf{e_1}\ \ \mathbf{e_2}\ \ \mathbf{e_3}) \tag{2.53}$$

with

$$\begin{aligned} \mathbf{e_1} &= \frac{1}{\sqrt{U^2+V^2+W^2}} \begin{bmatrix} U \\ V \\ W \end{bmatrix} \\ \mathbf{e_2} &= \frac{1}{\sqrt{U^2+V^2}} \begin{bmatrix} V \\ -U \\ 0 \end{bmatrix} \\ \mathbf{e_3} &= \mathbf{e_1} \times \mathbf{e_2} \end{aligned} \tag{2.54}$$

and then the transformed tensor, S'_{ij}, is given by

$$S'_{ij} = T_{ik} T_{jl} S_{kl} \tag{2.55}$$

Finally, the modified production rate is computed as

$$P_k = 2\nu_t S'_{ij} S'_{ij}, \quad \text{with} \quad S'_{ij} S'_{ij} = 0 \ \text{ if } \ i = j \tag{2.56}$$

Preliminary tests of this modification in two-dimensional computations of the stator vane geometry described in Section 1.4.4 showed significant improvements when compared with the use of the standard production rate expression. It was however not as efficient as the realizability contraint in reducing the overproduction of turbulence in the stagnation region. Thus it can be concluded that the erroneus predictions of P_k are not only due to the error in the irrotational strain contributions but are in part also caused by the mean shear contributions.

A Limit on the Production to Dissipation ratio

To prevent numerical oscillations in the iterative procedure towards a converged solution, Menter (1993) suggested that a limit on the production rate may be related to the computed dissipation rate according to

$$P_k \leq C_{lim}\, \varepsilon \tag{2.57}$$

with $C_{lim} = 20$. It was also argued that this limit eliminates the build-up of eddy-viscosity in stagnation regions. Later Menter *et al.* (2003) used a model

constant value of $C_{lim} = 10$ to improve the performance in stagnation regions. In both cases this limit was used together with the SST $k - \omega$ model described by Menter (1993). The limit may however be used with any turbulence model and it was therefore decided to compare this upper limit on P_k with the realizability constraint of Durbin (1995*b*) in other turbulence models and to find out what constant value will give reductions in growth comparable to the reductions of the realizability constraint. This study was carried out by Moran (2004), who computed an impinging jet flow and found that a value as low as $C_{lim} = 2.5$ was required to reduce the production in $v^2 - f$ model computations to about the same levels as achieved with the realizability constraint. It was also found that use of the realizability constraint produced somewhat better agreement with experimental data than did the upper limit of the production to dissipation ratio. Similar conclusions were also drawn by Narasimhamurthy (2004), who compared the two approaches in a turbulent trailing edge flow, containing perodic vortex shedding, computed with the low Reynolds number $k - \varepsilon$ model of Abe *et al.* (1994). It is worth noting that a reduction of the kinetic energy production was necessary to have any unsteady effect at all in the wake behind the trailing edge. The strong need to reduce the production in this flow was somewhat surprising, as this flow, when *averaged*, does not contain regions with strong irrotational strains.

Chapter 3

Numerical Method

3.1 The Solver CALC-BFC

CALC-BFC by Davidson & Farhanieh (1995) is a CFD code based on the finite volume discretization technique described in e.g. Versteeg & Malalasekera (1995). It solves the incompressible RANS equations for structured boundary fitted computational meshes of arbitrary shape. It employs the SIMPLEC pressure correction scheme and a co-located grid arrangement with Rhie and Chow interpolation. The Tri-Diagonal Matrix Algorith (TDMA) is used to solve the discretized set of equations in a segregated manner. For a more detailed description see Nilsson (2002), who added multi-block facilities to allow for large, parallel computations in complex domains. The exchange of information between the processors is handled using the Message Passage Interface, MPI.

In the discretization procedure it is assumed that the computational grid is orthogonal, i.e. that non-orthogonal contributions to diffusive fluxes can be neglected. This limitation should be of minor importance in the flows considered in this thesis. In the stator vane flow the grid is more or less orthogonal in regions where diffusion might be of importance, i.e. in the boundary layers. The asymmetric diffusor grid is close to orthogonal in the entire domain and the flat plate grid is orthogonal.

Several discretization schemes are available in CALC-BFC. For most of the computations the van Leer scheme, which is second order accurate except at local minima and maxima , was used in discretizing the momentum equations. No schemes of higher order have been tested, with the exception of the central differencing scheme used in Paper III, which is usually more accurate than the van Leer scheme even if it also is second order accurate. The equations governing the turbulence have been discretized with either the van Leer or the hybrid scheme, of

which the latter is first order accurate. The differences between the two schemes when used to discretize the turbulence equations have only had a minor influence on the converged solutions in the flows computed in this project.

Due to convergence problems, false time-stepping was often employed to enhance the numerical stability. The reasons for the poor convergence often encountered are believed to be: i) the use of the TDMA solver, which is not very sophisticated ii) the segregated solution procedure and iii) that, in computations in which the multi-block version has been used, the code is parallelized on a global level whereas the TDMA solver is not parallelized.

3.2 Numerical Domains

The Flat Plate Domain (Paper V)

This domain is straightforward and needs no further comments than those given in Paper V, where the grid is also plotted.

The Asymmetric Diffuser Domain (Paper III)

This mesh was generated with a FORTRAN code, specific for this particular geometry, written by D. D Apsley at the University of Manchester. The code generates a single block mesh with grid clustering by geometrical expansions and contractions in both the streamwise and cross-streamwise directions.

The Three-Dimensional Stator Vane Domain (Papers I and II)

The structured computational mesh was created using the ICEM pre-processor. This mesh generator is well suited for creating complex structured grids as the domain can be split into several subdomains in a top-down approach allowing for good control of each subdomain of the mesh. When the mesh is complete the subdomains can be clustered in larger blocks for output.

In most of the simulations the computational domain is a four block domain as illustrated in Figure 3.1. It consists of an O-grid around the stator vane, ensuring high quality cells in the important near wall region, onto which additional cells were added so that one period of an infinite row of stator vanes could be modelled (a part of the O-grid is included in block 2). As the experiment consisted of only two vane passages (cf. Figure 1.8) the assumption of the flow in the measurements being periodic can be questioned. It seems from measured velocities, however, that sufficiently good periodicity is achieved (Radomsky & Thole, 2000).

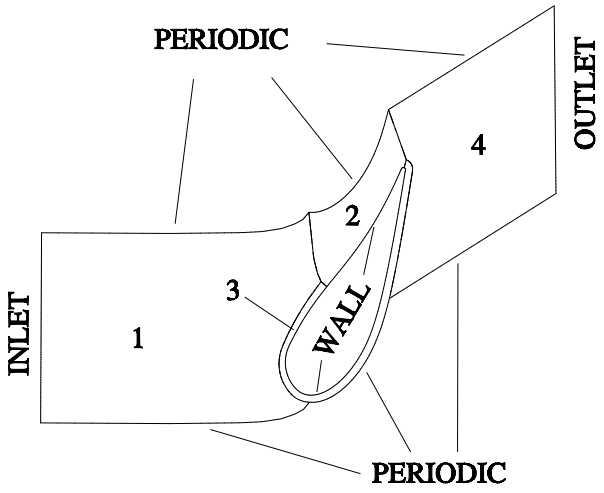

Figure 3.1: The computational domain with boundary conditions and block structure. The blocks are numbered from 1 to 4.

Also shown in Figure 3.1 are the boundary conditions. The inlet of the domain is located one chord length upstream of the stator vane stagnation point. This distance has been used by other investigators (Radomsky & Thole, 2000) and has proved to be sufficient. Finally, as the geometry is symmetric, only one half of the vane passage is analyzed and a symmetry boundary condition is applied at the vane midspan.

Figure 3.2 shows some regions of the grid in detail. It can be seen that use of the O-grid around the vane gives high quality cells close to the vane but there are some abrupt changes in e.g. cell size at block-to-block interfaces at various locations around the O-grid. This problem could in part have been solved by adding an additional O-grid around the present one. The additional outer O-grid could then have been stretched to fit the geometry between the two blades, whereas the inner O-grid would handle the near wall grid clustering. Using this approach the poor cell regions seen in Figure 3.2 could have been moved further out in the freestream, where gradients are generally lower.

3.3 Boundary Conditions

In the asymmetric diffuser all boundary conditions, with the exception of that for ε, which was analyzed in Section 2.4, are straightforward and are described in Paper III. In the flat plate computations there are some uncertainties regarding which boundary conditions to set to match the experimental set-up as closely as possi-

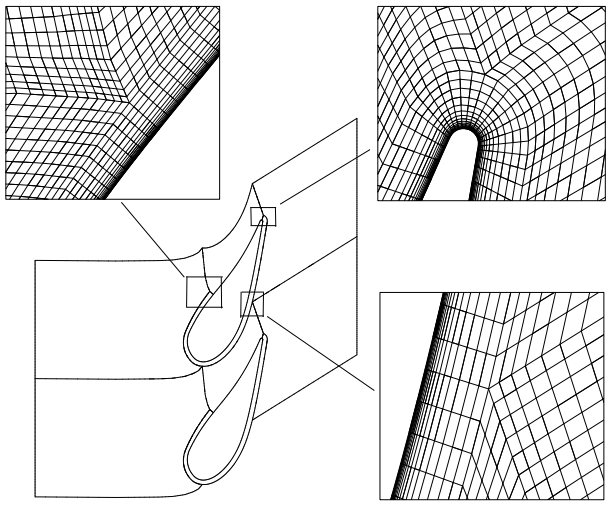

Figure 3.2: Some details of the computational grid. Note that two periods of the grid are shown, which illustrates the periodicity of the problem.

ble. These uncertainties are thoroughly discussed in Paper V. The only boundary conditions that need some further explanation are the inlet boundary conditions used in the stator vane computations.

3.3.1 Stator Vane Inlet Boundary Conditions

The possibly most uncertain boundary conditions to impose in RANS simulations of more complex flows are the inlet values of modelled turbulent quantities such as the turbulent kinetic energy, k, and its dissipation rate, ε. Ideally, all inlet values should be obtained in experiments in order to set up a numerical problem that is as close to reality as possible. The problem is that, in many experimental investigations, like the one used to validate the $v^2 - f$ model in this work, only some of the needed inlet profiles are available. For example, ε is very difficult to measure and is usually obtained via empirical relations to the turbulent length scale.

This work used another approach. As the flow entering the vane passage region has developed along a rather long splitter plate, it was assumed that the turbulence could be described accurately enough with the equations for fully developed channel flow. This allows for solving one-dimensional equations for the turbulent

quantities using the measured inlet velocity profile as input. These equations read

$$\begin{aligned} 0 &= \frac{\partial}{\partial y}\left(\left(\nu+\frac{\nu_t}{\sigma_k}\right)\frac{\partial k}{\partial y}\right)+P_k-\varepsilon \\ 0 &= \frac{\partial}{\partial y}\left(\left(\nu+\frac{\nu_t}{\sigma_\varepsilon}\right)\frac{\partial \varepsilon}{\partial y}\right)+\frac{C_{\varepsilon 1}P_k-C_{\varepsilon 2}\varepsilon}{\mathcal{T}} \\ 0 &= \frac{\partial}{\partial y}\left(\left(\nu+\frac{\nu_t}{\sigma_k}\right)\frac{\partial \overline{v^2}}{\partial y}\right)+kf-\frac{\overline{v^2}}{k}\varepsilon \\ L^2\frac{\partial^2 f}{\partial y^2}-f &= \frac{C_1-1}{\mathcal{T}}\left(\frac{\overline{v^2}}{k}-\frac{2}{3}\right)-C_2\frac{P_k}{k} \end{aligned} \tag{3.1}$$

where the dependence on the mean flow enters in the production term, P_k (cf. Eqn 2.8).

The validity of this method can be questioned as the inlet velocity profile is not fully developed. However, no other, more reliable way to provide the necessary inlet boundary conditions was found. The measured U profile and the generated k and $\overline{v^2}$ profiles are shown in Figure 3.3. It should be mentioned that the measured velocity profile is very different from fully developed channel flow and also quite different from standard zero pressure gradient boundary layer profiles (Kang *et al.* (1999) explained this by the presence of an adverse pressure gradient in the diffuser section of the wind tunnel). The mismatch between the measured and the fully developed velocity profile is responsible for the high levels of k in the boundary layer ($\sqrt{k}/u_* \approx 10$). Finally, note that the inlet boundary condition used for f is $\partial f/\partial n = 0$, where n is the normal unit vector of the inlet surface. Hence, no information on f is needed at the inlet.

3.4 Tri-Diagonal Matrix Algorithms (TDMA)

As mentioned earlier in this section, CALC-BFC uses a TDMA solver to iteratively solve the matrix equations that result from the discretization procedure. The standard CALC-BFC TDMA solver is of a segregated nature but, as it proved to be necessary to allow for coupled variable treatment at solid boundaries, a new coupled TDMA solver was implemented. This section describes both the segregated and the coupled solvers.

3.4.1 Segregated TDMA Solver

The structure of a tri-diagonal system of equations is given in Eqn 3.2.

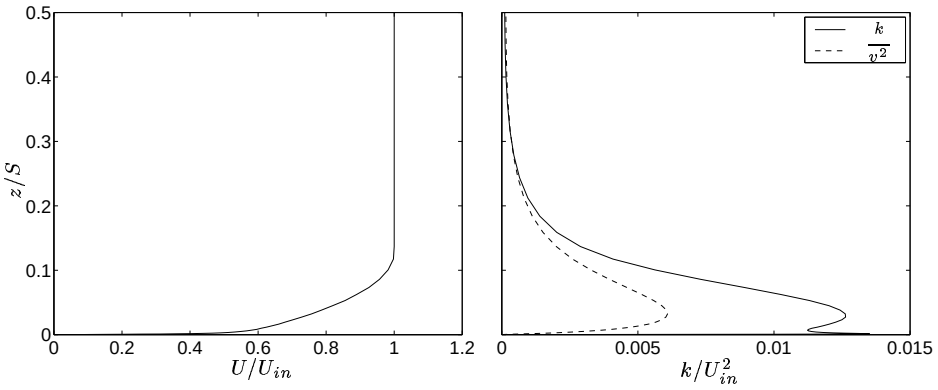

Figure 3.3: The profiles of U, k and $\overline{v^2}$ used as inlet boundary conditions. $u_*/U_{in} \approx 0.035$. The U profile was obtained from measurements while the k, v^2 and ε profiles were computed in a separate one-dimensional computation.

$$\begin{bmatrix} D_2 & -A_2 & 0 & \dots & & \\ -B_3 & D_3 & -A_3 & 0 & \dots & \\ 0 & -B_4 & D_4 & -A_4 & 0 & \dots \\ \vdots & \ddots & \ddots & \ddots & \ddots & \ddots \end{bmatrix} \begin{bmatrix} \phi_2 \\ \phi_3 \\ \phi_4 \\ \vdots \end{bmatrix} = \begin{bmatrix} C_2 + B_2\phi_1 \\ C_3 \\ C_4 \\ \vdots \end{bmatrix} \tag{3.2}$$

A TDMA solver is based on Gauss Elimination. The first step is to get rid of the left diagonal in the matrix, i.e. all the Bs, which means that the right diagonal and the load vector coefficients are modified according to Eqn 3.3 and 3.4 starting with the top row and then working through the matrix.

$$\begin{aligned} A_2^{mod} &= D_2^{-1} A_2 \\ C_2^{mod} &= D_2^{-1} \left[C_2 + B_2 \phi_1 \right] \end{aligned} \tag{3.3}$$

$$\begin{aligned} A_i^{mod} &= \left[D_i - B_i A_{i-1}^{mod} \right]^{-1} A_i \qquad i = 3, 4 \dots i_{max} - 1 \\ C_i^{mod} &= \left[D_i - B_i A_{i-1}^{mod} \right]^{-1} \left[C_i + B_i C_{i-1}^{mod} \right] \end{aligned} \tag{3.4}$$

After this operation the unknowns can be determined by recursive use of equation

$$\phi_i = C_i^{mod} + A_i^{mod} \phi_{i+1} \tag{3.5}$$

3.4.2 Coupled TDMA Solver

To enhance numerical stability it is sometimes beneficial to solve the equations coupled. The coupled equations approach enables implicit formulation of, for example, boundary conditions, where one flow field variable can be expressed in terms of another variable. An example is the boundary condition for f in the turbulence model suggested by Durbin (1995*b*)

$$f_{\text{wall}} = \frac{-20\nu^2}{\varepsilon}\left(\frac{v^2}{y^4}\right)_{\text{wall}} \tag{3.6}$$

In this expression for the wall value of f we see a coupling with two other flow field variables (if ν is a constant). When using the standard segregated approach where v^2 and ε have been recalculated separately a change in v^2/ε is multiplied by a factor of $-20\nu^2/y^4$. In the vicinity of wall boundaries the latter quantity is in my computations in the order of 10^{13} and it is obvious that even a small change in v^2/ε undergoing this strong amplification can lead to oscillations, or worse, divergence in the f-equation.

Now imagine that the v^2 and f sets of equations are combined into one system of equations. This allows implicitly removing the sensitivity of f at boundaries to changes in v^2 by adding coefficients in the left hand side matrix. The new, larger matrix is arranged as described in Eqn 3.7 (suggested by Eriksson (2002)) for a TDMA sweep in the i-direction without introducing any coupling between v^2 and f (for definitions of coefficients a_P, a_W, ... see Versteeg & Malalasekera (1995)).

$$\begin{bmatrix} a_{P2_{v^2}} & 0 & -a_{E2_{v^2}} & 0 & \dots & & \\ 0 & a_{P2_f} & 0 & -a_{E2_f} & 0 & \dots & \\ -a_{W3_{v^2}} & 0 & a_{P3_{v^2}} & 0 & -a_{E3_{v^2}} & 0 & \dots \\ 0 & -a_{W3_f} & 0 & a_{P3_f} & 0 & -a_{E3_f} & \\ \vdots & \ddots & \ddots & \ddots & \ddots & \ddots & \ddots \end{bmatrix} \begin{bmatrix} v_2^2 \\ f_2 \\ v_3^2 \\ f_3 \\ \vdots \end{bmatrix} = \begin{bmatrix} c_{2_{v^2}} + a_{W2_{v^2}} v_{wall}^2 \\ c_{2_f} + a_{W2_f} f_{wall} \\ c_{3_{v^2}} \\ c_{3_f} \\ \vdots \end{bmatrix} \tag{3.7}$$

Now the f boundary condition and the source term in the v^2 equation can be introduced implicitly. For example, if our $i = 1$ boundary is a wall, we can implement the boundary condition given by Eqn 3.6 by adding coefficient F_{bc} at

the matrix position giving the connection of the first interior f value with the f wall value. Implicit treatment of source term $-kf$ in the v^2 equation corresponds to adding coefficient S_{v^2}. F_{bc} and S_{v^2} are given by Eqn 3.8

$$\begin{aligned} F_{bc} &= \frac{20\nu^2}{\varepsilon x_n^4} a_{2W_f} \\ S_{v^2} &= -\rho k V \end{aligned} \tag{3.8}$$

$$\begin{bmatrix} a_{P2_{v^2}} & S_{v^2} & -a_{E2_{v^2}} & 0 & \dots & & \\ F_{bc} & a_{P2_f} & 0 & -a_{E2_f} & 0 & \dots & \\ -a_{W3_{v^2}} & 0 & a_{P3_{v^2}} & S_{v^2} & -a_{E3_{v^2}} & 0 & \dots \\ 0 & -a_{W3_f} & 0 & a_{3P_f} & 0 & -a_{E3_f} & \\ \vdots & \ddots & \ddots & \ddots & \ddots & \ddots & \ddots \end{bmatrix} \begin{bmatrix} v_2^2 \\ f_2 \\ v_3^2 \\ f_3 \\ \vdots \end{bmatrix} =$$

$$= \begin{bmatrix} c_{2_{v^2}} + a_{W2_{v^2}} v_{wall}^2 \\ c_{2_f} \\ c_{3_{v^2}} \\ c_{3_f} \\ \vdots \end{bmatrix} \tag{3.9}$$

This approach has two main disadvantages. The memory requirement increases as we must be able to handle matrices of size $2i_{max}$ by $2i_{max}$ instead of i_{max} by i_{max}. The other drawback is that the matrix is now penta diagonal, which means that it is not possible to use a standard TDMA solver. Not much can be done to deal with the first problem, whereas it is fairly easy to rewrite a TDMA solver so that it can handle penta diagonal systems of equations. This is done by changing the *scalar* coefficients in the standard TDMA matrix (Eqn 3.2) to *two by two matrices* and the unknown variable values and the load vector values to vectors of two elements. In this way we get exactly the same structure of the TDMA matrix and can adopt the same solution methodology as for the scalar (special) case with the only difference that all operations are now matrix or vector operations. This is also the reason why, for example, D_2/A_2 in Eqn 3.3 is written in the more general form $A_2^{-1}D_2$. The arrangement of the coefficients for the new TDMA matrix equation is given in Eqn 3.10 and 3.11.

$$
\begin{aligned}
D_2 &= \begin{bmatrix} a_{P2_{v^2}} & S_{v^2} \\ F_{bc} & a_{P2_f} \end{bmatrix} \\
D_i &= \begin{bmatrix} a_{Pi_{v^2}} & S_{v^2} \\ 0 & a_{Pi_f} \end{bmatrix}, \quad i > 2 \\
A_i &= \begin{bmatrix} a_{Ei_{v^2}} & 0 \\ 0 & a_{Ei_f} \end{bmatrix} \\
B_i &= \begin{bmatrix} a_{Wi_{v^2}} & 0 \\ 0 & a_{Wi_f} \end{bmatrix}
\end{aligned} \tag{3.10}
$$

$$
\phi_i = \begin{bmatrix} v_i^2 \\ f_i \end{bmatrix}, \qquad C_i = \begin{bmatrix} c_{i_{v^2}} \\ c_{i_f} \end{bmatrix} \tag{3.11}
$$

3.5 Notes on the Commercial Software Used

Throughout the work here the computations made with the in-house code CALC-BFC have occasionally been complemented with computations performed with the Fluent commercial software. There are several benefits in taking this approach and the effort needed to get acquainted with an additional software was considered worthwhile. The complementary use of a commercial software allowed establishing a database with results for a wide range of commonly used turbulence models, whose implementations have been extensively benchmarked against experiments in a wide range of flow conditions. Parts of this set of data have been published in Papers I & II to give an overview of the performance of different turbulence models in the flow considered. Another opportunity was the possibility to use an early version of the $v^2 - f$ turbulence model that had been implemented in Fluent by the use of so called User-Defined Functions (subroutines). The imlementation employed was a trial version of the CASCADE Technologies Inc. V2F$^{\mathrm{TM}}$ module for Fluent 5. The use of this module allowed comparison of the results of exactly the same turbulence model (the $v^2 - f$ model) on exactly the same computational grid with exactly the same boundary conditions using two different CFD codes. The numerical features (e.g. solver and disctretization scheme) of the two codes were chosen to be as equal as possible. Results of this comparison are also included in Papers I & II. The comparison would of course also instantly reveal any severe error in the implementation of the $v^2 - f$ model in the CALC-BFC code.

A final purpose of using a commercial software was to increase the availability of recent progress in, for example, turbulence model development to the industrial partners involved in this project. The reason behind industry's dissatisfaction was

of course that any model development carried out within the project would not be available until the research community accepted the new ideas and the distributors of the specific CFD code used implemented them in their software. And, when finally available, the ideas are also available to any competitor using the same software. To illustrate the potential of overcoming this problem using User-Defined Functions, a version of the $v^2 - f$ model was implemented in Fluent using this approach and distributed to the partners involved.

Chapter 4

Summary of Papers

4.1 Paper I

This paper was based on a contribution to the 4^{th} International Symposium on Turbulence, Heat and Mass Transfer held in Antalya, Turkey, 2003. It was later, together with some 25 other contributions, selected for publication in an Int. Journal of Heat and Fluid Flow Special Issue.

4.1.1 Background

Early in this project it was decided to implement the v^2-f model in the CFD code described in Section 3 and evaluate its performance in a gas turbine stator vane flow. The progress was initially very slow as it proved difficult to get the computations with the new turbulence model running smoothly. As the respondent was fairly new in the area of turbulence modelling it was hard to pinpoint the direct cause of the problems encountered. Were they due to errors in the numerical grid? Or, which was more likely, errors in the implementation of the new model? It eventually turned out to be neither of these candidates. Instead it was the formulation of the model itself that was not at all stable, at least not when used in the CALC-BFC framework. After about three months of debugging it was realized that the numerics could be substantially improved by avoiding the use of the realizability constraint in the f equation. The motivation for Paper I was therefore to analyze why the realizability could have such a strong influence on the numerical properties and, more importantly, how strongly the results of the v^2-f model depend on the use of the same constraint. A second purpose was to compare two different versions of the v^2-f model to see whether the modified version given in e.g. Lien & Kalitzin (2001) gave the same results as the original version of the

model.

4.1.2 Discussion of Results

As mentioned, it was found that the use of the realizability constraint on the turbulence time scale can cause problems when used in the f equation. The reason was attributed to a positive feedback loop where a decrease in the time scale given by the realizability constraint led to an increase in the modelled production of v^2, which further reduced the upper bound on the time scale. Three alternative routes to using the realizability constraint in the f and v^2 equations, where one was not to use it at all, were tested and all proved to improve the numerical stability of the model. It was also shown, by applying several modified formulations of the realizability constraint, that its use in the v^2 and f equations, at least in the flow computed, had only a minor influence on the converged solution.

Further, the effect of the model constant, C_{lim} (cf. Eqn 2.43), introduced together with the realizability constraint was investigated. By tuning this constant against measured turbulence kinetic energy profiles it was found that a value of 0.6 gave the overall best agreement. This was very satisfying since this is the same value that has been found suitable by other authors, which suggests some universality of this constant.

Finally, it was shown that the original version of the $v^2 - f$ model, i.e. the version with the numerically cumbersome f wall boundary condition, produced the overall best agreement with experimentally obtained stator vane heat transfer data.

4.2 Paper II

This paper was based on a contribution to the TURBO EXPO Conference in Vienna, Austria, 2004. It was later, by people involved in the organization of the conference, recommended for publication in ASME Journal of Turbomachinery.

4.2.1 Background

The motivation for this paper is the true motivation as to why the stator vane flow was to be computed with the $v^2 - f$ model in the first place (Paper I may be considered more of a side track). That is, we were interested in the model's performance in a complex flow not too different from real flows found in gas turbine engines. Again, both versions of the $v^2 - f$ model were considered. A second objective was to improve the understanding of the secondary flow mechanism responsible

for the strong increase in endwall heat transfer in the passage between two stator vanes. Also of interest was the response of the model's heat transfer predictions to increased levels of freestream turbulence. Two-dimensional midspan computations were performed for this purpose. The evaluation was to be done by: i) comparing the computed results with experimental data of Kang & Thole (2000) and ii) comparing the models' performance with that of turbulence models available in the Fluent commercial software. At the time these computations were performed Fluent had just released a $v^2 - f$ module of their own that was made available for testing at VAC.[1] A problem with the module was that the details of that particular version of the $v^2 - f$ model were never given, which of course was rather annoying, especially since there had been so many difficulties in getting the model to work in the CALC-BFC code. Nevertheless, here was an opportunity to identify which version of the $v^2 - f$ model the Fluent module actually solved, *and* to compare the performance of our in-house code with the commercial code using exactly the same grid and the same (?) turbulence model. Note that today Fluent give the details of the model they have implemented. They may be found in Cokljat *et al.* (2003).

4.2.2 Discussion of Results

It was found that the two versions of the $v^2 - f$ model gave very similar results, particularly in terms of predicting the secondary flow originating from the vane/endwall junction, known as the horseshoe vortex system. The $v^2 - f$ model was found to be able to predict the presence of some of the vane passage vortices but in general gave somewhat too low intensities of the swirling motion as compared with experimental data. A very close coupling between the endwall heat transfer and the secondary motion was illustrated. The heat transfer predictions with both versions of the model responded fairly accurately to increases in freestream turbulence intensity, with the original model performing somewhat better in the vane stagnation midspan region.

Of the models available in Fluent, the $v^2 - f$ model, followed by the RNG $k - \varepsilon$ model, was found to give the best agreement with measurements. The poorest results in terms of predicting the secondary flow were obtained with the Realizable $k - \varepsilon$ model. It was also found that the Fluent $v^2 - f$ version and the versions implemented in CALC-BFC gave almost identical results, which was an encouraging result. Further, it was illustrated that turbulence models without a fix for

[1] All the Fluent computations were performed at Volvo Aero Corporation, Trollh¨attan, Sweden, and the respondent wishes to acknowledge Dr. Jonas Larsson who made the time spent at VAC a very valuable experience.

the stagnation point anomaly, including the $v^2 - f$ with the realizability constraint deactivated, suffer from massive overpredictions in stagnation point regions. One example of a model that failed in this aspect was the Fluent implementation of the SST $k - \omega$ model. According to Dr. Fredrik Carlsson, Fluent, Sweden (private communication), this problem has been dealt with in the latest version of Fluent.

Finally, the FLUENT predictions of the endwall stagnation region heat transfer were compared with experiments. All models gave similar estimates of the heat transfer in the region upstream of the vane. As the vane is approached, the influence of the horseshoe vortex, which significantly increases the heat transfer to the endwall, is clear. It was found, however, that when the intensity of the predicted vortex was close to the measured data the models tended to overpredict the heat tranfer to the endwall. This, and the fact that the measured heat transfer signature of the vortex was not as clear in the experimental data as in the computations, suggests that the measured heat flux signal might have been affected by heat leakage within the endwall or that the measured flow field was unsteady. Both phenomena would smear out the measured heat transfer profile.

Finally, the endwall stagnation region heat transfer results also suggest that the model implemented in Fluent was very similar to the modified version of the v^2-f model (the version with a stable f wall boundary condition). The results of these two implementations produced an almost perfect match, whereas the original $v^2 - f$ model captures the heat transfer somewhat better.

4.3 Paper III

This paper is a modified and substantially extended version of a contribution to the Turbulence Shear Flow Phenomena in Williamsburg, USA, 2005, now submitted to the International Journal of Heat and Fluid Flow.

4.3.1 Background

Predicting separated flows with eddy-viscosity based closures is difficult. One such flow that has been extensively studied is the asymmetric diffuser first considered by Obi *et al.* (1993). The main reason why it is commonly used as a test case for turbulence models is its well-defined boundary conditions and its apparent simplicity. The flow physics is all but simple, however, and constitute an exceptionally difficult test case. In spite of the fact that the flow has been computed by a number of CFD researchers, the underlying reason as to why it is so difficult to predict using RANS closures is not well understood. Some studies have suggested that the near wall behavior is of great importance (e.g. Apsley &

Leschziner, 1999), which suggests that the ability of the $v^2 - f$ model to represent nonlocal wall effects might be decisive. The main purpose of this study was to shed additional light on the subject and to identify the flow features that are of dynamic importance. The LES data of Kaltenbach *et al.* (1999) were used for validation purposes.

Even though the $v^2 - f$ model has shown promising results in this flow, it is in principle unable to account for turbulence anisotropy. It was therefore decided to investigate the performance of the nonlinear extension to the $v^2 - f$ model suggested by Pettersson-Reif (2000). Note that the nonlinear model has proved capable of accurate predictions of anisotropy driven effects and that it is of interest to investigate whether the extended model still performs as well in separated flows as the less sophisticated linear model.

4.3.2 Discussion of Results

This study showed that the dynamically most important flow region is the near wall region in close vicinity to the diffuser entrance. Here exists a delicate balance between the Reynolds stresses and it is required that the evolution of all three components ($\langle u^2 \rangle$, $\langle v^2 \rangle$ and $\langle uv \rangle$) is correctly modelled. Several interesting observations were made. One was that the reason why the linear $v^2 - f$ model gets this flow about right is not that it is particularly good, but rather that it produces two errors that happen to cancel each other. Another was that the nonlinear $v^2 - f$ model, at least in the beginning of the diffuser, did a very good job in representing the complex flow anisotropy, but did substantially worse than the linear model in terms of mean velocity profiles. The reason for this puzzling result turned out to be that one of the errors the linear model produced was improved a great deal with the consequence that the other error was left unbalanced.

It was also shown that the performance of the nonlinear model could be improved with a slight modification of the $C_{\varepsilon 1}$ coefficient. This modification seemed also to fix the unbalanced error. It could therefore also be concluded that the nonlinear constitutive equation suggested by Pettersson-Reif (2000) is sufficiently accurate for the purpose of computing the complex flow field in the asymmetric diffuser.

The effect of a more elaborate turbulence diffusion model in the k and ε equations was also tested, and the results seem to suggest that the turbulence transport model does not play a primary role in this particular flow and that the k and ε equations are dominated by their source terms.

A final conclusion was that the flow in the asymmetric diffuser, at least in the first half of the diffusing section, is largely of a parabolic nature. A consequence is that errors in the early part of the diffuser rather severely affect the flow de-

velopment in downstream portions of the diffuser. It seems thus to be of little value to optimize a turbulence model to perform well in the separated region of the diffuser if the upstream flow is not correctly captured.

4.4 Papers IV and V

4.4.1 Motivation

The $v^2 - f$ model, as almost every other turbulence model, is known to predict transition too early. Therefore, in an effort to increase the $v^2 - f$ model's reliability as a gas turbine design tool, the overall aim of Papers IV-V was to identify a measure to improve its performance in transitional flows.

Paper IV is a review of transitional modelling that includes a variety of approaches to the problem suggested in the second half of the 20th century. As by-pass transition is probably the transition mode that suits a statistical modelling approach best, this mode, and its modelling, is the one that is most thoroughly discussed. Included are also the latest findings on the nature of by-pass transition. The main purpose of the review was to search the existing literature for a modelling approach that could be coupled to the, in fully turbulent flows, reasonbly accurate $v^2 - f$ turbulence model. A second purpose was of course to provide a reference text where most relevant earlier work on the subject is collected.

4.4.2 Discussion of Results

It was decided to adopt the modelling concept of Mayle & Schultz (1997), refined by Walters & Leylek (2004), i.e. to introduce an additional transport equation governing the evolution of a laminar kinetic energy. It is well known that streaks of laminar u-component fluctuations are somehow created in the pretransitional boundary layer and that these streaks are precursors to the formation of turbulent spots. It was thus believed that modelling statistics of these streaks (their fluctuating energy) would be an approach to modelling transitional phenomena that stood on a reasonably firm ground. The coupling of most of the concepts introduced by Walters & Leylek (2004) with a modified version of the $v^2 - f$ model is what Paper V is about.

This work has led to the conclusion that the model of Walters & Leylek (2004) is very sensitive; the freestream turbulence length scale and a few of their concepts have to be reconsidered.

Chapter 5

Concluding Remarks

This thesis has dealt with the closure, or modelling, of turbulence transport effects on averaged flow properties of turbulent flows. The main applications have all been related to turbomachinery components with a focus on flow or modelling features particularly important to heat transfer in gas turbine engines. The most important findings will be given below in three separate sections. Section 5.1 summarizes the results of the two and three-dimensional computations reported in Papers I & II. Also included in this section are the results of the realizability constraint study and a few comments on the present computational approach in general. Section 5.2 gives some comments on the potential of using nonlinear eddy-viscosity models together with findings on the subtle subject of turbulence modelling in separating flows. Section 5.3 is a summary of the conclusions drawn in the effort to improve the transition modelling capability of the $v^2 - f$ turbulence model. The final section contains some guidelines for future work in the area of turbulence modelling for gas turbine applications.

5.1 Stator Vane Passage Flows

Two-dimensional Passage Flow Computations

All computations of the two-dimensional stator vane flow produced attached velocity fields with very small overall differences in behavior among the different turbulence models investigated. The largest differences are found within the boundary layers. More specifically, the flow property that differs the most is the location of transition onset. It was found that no model was able to predict the onset location but, by judging the performance in terms of heat transfer predictions, the $v^2 - f$ model of Durbin (1995*b*) must be regarded as the most reliable model.

In stagnation point flows it is important that the model used for turbulence closure is able to handle the so called stagnation point anomaly (large overprediction of turbulence kinetic energy). Models that do not handle this problem predict too high heat transfer rates and the elevated levels of turbulence tend also to accelerate the laminar to turbulence transition process. It was found that an efficient way to reduce the erroneous growth of fluctuating energy was to employ the realizability constraint of Durbin (1995*a*). However, this constraint, when expressed in terms of an upper bound on the turbulence time scale, proved to destabilize the path to a converged solution. A mechanism behind the instabilities was suggested together with some alternative ways to employ the constraint that all improved the numerical stability. The most straightforward alternative to reduce the overprediction of turbulent kinetic energy is simply to express the constraint in terms of a bound on the predicted eddy-viscosity.

Three-dimensional Passage Flow Computations

The three-dimensional computations of the stator vane passage flow illustrated the crucial dependence of endwall heat transfer on the secondary flow structures emanating from the stator vane/endwall junction. The origin of these so called horseshoe vortices is the vorticity contained in the oncoming boundary layer. In the flow computed, the boundary layer is thick, which causes strong secondary motions. It therefore turned out that accurately capturing the roll-up of these vortices is particularly important. The presence of this vortex causes the relatively thick oncoming boundary layer to separate from the endwall. This is unfortunate since the boundary layer fluid should act as an insulating layer, protecting the endwall from the hot freestream fluid. The vortex also effectively replaces the boundary layer fluid (that separated from the endwall) with hot fluid from the freestream that, owing to the rotating motion of the vortex, impinges on the endwall surface which severely increases the rate of heat transfer to the endwall.

The results thus indicate that the endwall heat transfer rate primarily depends on a correct prediction of the secondary flow structures present. Of secondary importance is the prediction of the heat transfer due to turbulence[1]. However, of crucial importance is the effect of turbulence on the secondary flow field. That is, if for some reason the predicted effect of turbulence erroneously affects the secondary motion, this error will also ruin the heat transfer prediction in the vane passage.

Of the different turbulence models investigated, the two versions of the $v^2 - f$ model tested performed better than the turbulence closures available in the Fluent

[1]This was also verifi ed by varying the inlet turbulence boundary conditions which only slightly modifi ed the computed heat transfer data.

commercial software with the possible exception of the RNG $k-\varepsilon$ model. It was also found that the in-house CALC-BFC code and the trial version of a v^2-f module (cf. Section 3.5) implemented with User-Defined Functions gave identical results. That is, with the same turbulence model, the same numerical grid and boundary condition, CALC-BFC and Fluent give identical results. Finally, of the two versions of the v^2-f model tested in this flow, the version in Durbin (1995*b*) did somewhat better in terms of heat transfer, a trend also seen in the two-dimensional vane computations. Both models, however, perform less satisfactorily, as compared with the results in the stagnation region, some distance into the stator vane passage. It is believed that this is due to an inaccurate representation of the secondary vortices as they are convected through the vane passage. In all computations the intensity of the secondary motions and the net flow towards the suction side of the adjacent stator vane were underpredicted.

All v^2-f model computations performed with the in-house CALC-BFC code were problematic from a numerical stability point of view. The main source of instability is believed to be the f equation, which is an equation of an elliptic nature describing the evolution of a turbulence quantity with large source terms creating a strong coupling to other turbulence quantities. There is thus room for oscillations not seen in the other turbulence equations that are not convected through the numerical domain.

In the computations made with the Durbin (1995*b*) model the stability problems were even worse owing to the extremely strong coupling of the f wall boundary condition to other near wall turbulence quantities. These computations were never even close to converging without the use of the coupled TDMA solver described in Section 3.4.2[2]. With the coupled solver the stability of the Durbin (1995*b*) model was improved and the code behaved as when the modified more stable version of the v^2-f model was used. There was initially some hope that the coupled solver would also improve the stability of the code-friendly version of the v^2-f model, as this solver allows implicit treatment of the v^2 equation source term (kf) and the k equation sink term ($-\varepsilon$), but no conclusions on decisive improvements could be drawn. It is interesting to note, however, that the code-friendly version of the v^2-f model seems not to have any additional numerical difficulties, as compared with other turbulence models available, when implemented in Fluent.

[2]This model was also implemented in Fluent (version 6.2.16) using User-Defi ned Functions and did, after considerable effort, produce a converged solution for a one-dimensional, fully developed channel fbw computation. The stability seems however not to be signifi cantly better than with the CALC-BFC solver.

5.2 Separation in the Asymmetric Diffuser

The linear $v^2 - f$ model is argued to be among the better models in flows involving separation. It is however unable to make correct representations of turbulence anisotropy. In this study the potential of using a nonlinear eddy-viscosity turbulence model was therefore investigated. The model tested was the nonlinear extension to the $v^2 - f$ model suggested by Pettersson-Reif (2000). When compared with the linear version of the model, all the components of the Reynolds stress tensor, and especially its normal components, were substantially improved in almost the entire numerical domain. On the other hand, the prediction of the mean flow was worse than with the linear model. This somewhat surprising finding, given the quality of the Reynolds stresses, could be explained in a careful analysis of the momentum equation source terms, i.e. the Reynolds stress derivatives, in the close vicinity of the curved wall in the diffuser entrance region. Here a delicate balance between the Reynolds stresses exists and it turned out that the reason why the linear model produced results in close agreement with LES data was that two errors of equal magnitude cancelled each other. The nonlinear extension proved to solve one of the two problems, which left the other error unbalanced.

A few modifications to the nonlinear model were preliminarily assessed in an effort to further improve its performance. All modifications involved changes of the ε equation coefficient $C_{\varepsilon 1}$, which controls the production rate of ε. One of the modifications tested was found to significantly improve the model performance in the diffuser entrance and also improved the predicted mean velocity field. This modification reduced the unbalanced near wall error mentioned above, which further supports our reasoning that the near wall behavior is of utmost importance to the flow in the diffuser.

Finally, it was concluded that the choice of diffusion model for the turbulence kinetic energy and its dissipation rate was of subordinate importance and, thus, that these equations are dominated by their source terms in the asymmetric diffuser flow.

5.3 Transition

The subject of transition modelling was reviewed in Paper IV. The main purpose of that study was to examine existing ideas and to find a basis for extending the capabilities of the $v^2 - f$ model to also include transitional flows. After considering a few concepts in more detail it was decided to adopt the modelling framework suggested by Walters & Leylek (2004). Here an additional transport equation for a laminar kinetic energy is solved together with a typical turbulence model. Walters

& Leylek (2004) use a two-equation $k - \varepsilon$ model for turbulence closure and the idea here was simply to adapt the ideas to the $v^2 - f$ model framework.

Before coupling the laminar kinetic energy approach to the $v^2 - f$ model, the original model of Walters & Leylek (2004) was examined by computing the fully developed turbulent channel flow and some transitional flows over a flat plate. The same test cases as considered in Walters & Leylek (2004) were computed and their results were successfully reproduced. However, when a different set of experimental data, the ERCOFTAC T3A and T3B test cases, was considered it was found that the Walters & Leylek (2004) model was extremely sensitive to the length scale in the freestream. For this set of data the turbulence length scale in the freestream was smaller than in the flat plate test case used by Walters & Leylek (2004), which caused the model to behave erroneously. For example, it predicted an earlier transition onset location for the T3A case (3% freestream turbulence intensity) than for the T3B (6% freestream turbulence intensity) case. A mechanism behind this fallacious behavior was suggested together with a measure to correct it to be used in the adaption to the $v^2 - f$ model.

The adaption of the laminar kinetic energy approach to the $v^2 - f$ model required several modifications in addition to the new transport equation added. One was a modification of the dissipation rate equation, which now governs the modified quantity $\tilde{\varepsilon}$, defined as $\varepsilon = \tilde{\varepsilon} + D$, where the D term is the very near wall dissipation rate. The most problematic issue was to find a measure to reduce the production rate of turbulent kinetic energy in the pretransitional region without modifying the $v^2 - f$ model's behavior in fully turbulent boundary layers. A damping function dependent on the ratio of a turbulence and a mean flow time scale and the ratio of the total fluctuating energy and the laminar fluctuating energy was suggested and preliminarily assessed.

The new model suggested in Paper V needs further validation but has been shown to capture the main features of the development of the statistics of the laminar fluctuations that are precursors to the onset of transition to turbulence.

5.4 Suggestions for Future Work

The work carried out in this project has illustrated the potential of the eddy-viscosity based $v^2 - f$ turbulence model. As the model was able to handle the very different, and very complex, flows in both the three-dimensional stator vane passage flow and the flow in the asymmetric diffuser with reasonable success, this turbulence model is likely to be among the more reliable models in other complex flows as well. In flows in which separation is present and in flows where heat transfer is of primary interest, the $v^2 - f$ model is believed to offer advantages

over other eddy-viscosity based closures.

There appears, however, to exist two weaknesses in the model. It is more or less unable to account for turbulence anisotropy and predicts the onset of transition to occur too early. Both problems have been addressed in this thesis. The nonlinear extension to the $v^2 - f$ model appears to offer substantial improvements in the representation of turbulence anisotropy. However, two important weaknessess of the nonlinear model have been pinpointed and need further attention. One is the modelling of the dissipation rate equation. A modification that improved the model's performance has beed suggested but needs to be more extensively tested in other applications. The other is that the nonlinear terms added tend to make the model numerically unstable. A continuation of the development of the nonlinear model will therefore require implementation of state-of-the-art numerical methods to increase the model's reliability.

The subject of transition is of crucial importance to the design of turbomachinery components, especially those for which heat transfer is of primary importance, and cannot be neglected. The effort described here to improve the $v^2 - f$ model's performance in transitional flows needs further work on both model development and validation. Of the two 'missing links', that of transition is by far the most important to turbomachinery design.

Bibliography

ABE, K., KONDOH, T. & NAGANO, Y. 1994 A new turbulence model for predicting fluid flow and heat transfer in separating and reattaching flows–1. Flow field calculations. *Int. J. of Heat and Mass Transfer* **37**, 139–151.

APSLEY, D. & LESCHZINER, M. 1999 Advanced turbulence modelling of separated flow in a diffuser. *Flow, Turbulence and Combustion* **63**, 81–112.

BATCHELOR, G. K. 1967 *An introduction to fluid dynamics*. Cambridge University Press.

BOYLE, R. & RUSSELL, L. 1990 Experimental determination of stator endwall heat transfer. *Journal of Turbomachinery* **112**, 547–558.

BRADSHAW, P. 1996 Turbulence modelling with application to turbomachinery. *Proc. Aerospace Science* **32**, 575–624.

COKLJAT, D., KIM, S., IACCARINO, G. & DURBIN, P. 2003 A comparative assessment of the $\overline{v^2} - f$ model for recirculating flows. AIAA-2003-0765.

CRAFT, T. J. 2002 Modelling of separating and impinging flows. In *Closure Strategies for Turbulent and Transitional Flows* (ed. B. E. Launder & N. D. Sandham), pp. 341–360. Cambridge University Press.

DALY, B. J. & HARLOW, F. H. 1970 Transport equations in turbulence. *International Physics of Fluids* **13**, 2634–2649.

DAVIDSON, L. & FARHANIEH, B. 1995 CALC-BFC: A finite-volume code employing collocated variable arrangement and cartesian velocity components for computation of fluid flow and heat transfer in complex three-dimensional geometries. Rept. 95/11. Dept. of Thermo and Fluid Dynamics, Chalmers University of Technology, Gothenburg.

DUNN, M. 1990 Phase and time-resolved measurements of unsteady heat transfer and pressure in a full-stage rotating turbine. *Journal of Turbomachinery* **112**, 531–538.

DUNN, M., RAE, W. & HOLT, J. 1984 Measurement and analyses of heat flux data in a turbine stage: Part ii—discussion of results and comparison with predictions. *Journal of Engineering for Gas Turbines and Power* pp. 234–240.

DURBIN, P. 1991 Near-wall turbulence closure modeling without 'damping functions'. *Theoretical and Computational Fluid Dynamics* **3**, 1–13.

DURBIN, P. 1993 Application of a near-wall turbulence model to boundary layers and heat transfer. *International Journal of Heat and Fluid Flow* **14**, 316–323.

DURBIN, P. 1995*a* On the $k - \varepsilon$ stagnation point anomaly. *International Journal of Heat and Fluid Flow* **17**, 89–90.

DURBIN, P. 1995*b* Separated flow computations with the $k - \varepsilon - v^2$ model. *AIAA Journal* **33**, 659–664.

ERIKSSON, L. 2002 private communication. Dept. of Thermo and Fluid Dynamics, Chalmers University of Technology, G¨oteborg, Sweden.

GIEL, P., FOSSEN, R. V., BOYLE, R., THURMAN, D. & CIVINSKAS, K. 1999 Blade heat transfer measurements and predictions in a transonic turbine cascade. NASA/TM—1999-209296.

GIEL, P., THURMAN, D., FOSSEN, R. V., HIPPENSTEELE, S. & BOYLE, R. 1998 Endwall heat transfer measurements in a transonic turbine cascade. *Journal of Turbomachinery* **120**, 305–313.

GIEL, P., THURMAN, D., LOPEZ, I., BOYLE, R., FOSSEN, R. V., JETT, G., CAMPERCHIOLI, T. & LA, H. 1996 Three-dimensional flow field measurements in a transonic turbine cascade. *ASME paper No. 96-GT-113* .

GRAZIANI, R., BLAIR, M., TAYLOR, J. & MAYLE, R. 1980 An experimental study of endwall and airfoil surface heat transfer in a large scale turbine blade cascade. *Journal of Engineering for Power* **102**, 257–267.

HARVEY, N., ROSE, M., COUPLAND, J. & JONES, T. 1999 Measuremement and calculation of nozzle guide vane end wall heat transfer. *Journal of Turbomachinery* **121**, 184–190.

HERMANSON, K. & THOLE, K. 2000*a* Effect of inlet conditions on endwall secondary flows. *Journal of Propulsion and Power* **16**, 286–296.

HERMANSON, K. & THOLE, K. 2000*b* Effect of Mach number on secondary flow characteristics. *International Journal of Turbo and Jet Engines* **17**, 179–196.

JOHANSSON, G. & KLINGMANN, J. 1994 An LDA based method for accurate measurements of the dissipation rate tensor with application to a circular jet. In *7th Int. Symp. on Applications of Laser Techniques to Fluid Mechanics*. Lisbon.

JOHANSSON, T. 2002 private communication. Dept. of Thermo and Fluid Dynamics, Chalmers University of Technology, G¨oteborg, Sweden.

JONES, W. & LAUNDER, B. 1972 The prediction of laminarization with a two-equation model of turbulence. *Int. J. of Heat and Mass Transfer* **15**, 301–314.

KALITZIN, G. 1999 Application of the $\overline{v^2} - f$ model to aerospace configurations. Center for Turbulence Research Annual Research Breifs.

KALTENBACH, H., FATICA, M., MITTAL, R., LUND, T. & MOIN, P. 1999 Study of flow in a planar asymmetric diffuser using large-eddy simulation. *Journal of Fluid Mechanics* **390**, 151–185.

KANG, M., KOHLI, A. & THOLE, K. 1999 Heat transfer and flowfield measurements in the leading edge region of a stator vane endwall. *Journal of Turbomachinery* **121**, 558–568.

KANG, M. & THOLE, K. 2000 Flowfield measurements in the endwall region of a stator vane. *Journal of Turbomachinery* **122**, 458–466.

KATO, M. & LAUNDER, B. 1993 The modelling of turbulent flow around stationary and vibrating square cylinders. In *Ninth Symposium on Turbulent Shear Flows*, pp. 10–4–1–10–4–6.

LANGSTON, L., NICE, M. & HOOPER, R. 1977 Three-dimensional flow within a turbine cascade passage. *Journal of Engineering for Power* **99**, 21–28.

LAUNDER, B., REECE, J. & RODI, W. 1975 Progress in development of a Reynolds-stress turbulence closure. *Journal of Fluid Mechanics* **68**, 537–566.

LIEN, F. & KALITZIN, G. 2001 Computations of transonic flow with the $\overline{v^2}$-f turbulence model. *International Journal of Heat and Fluid Flow* **22**, 53–61.

MANCEAU, R., WANG, M. & LAURENCE, D. 2001 Inhomogeneity and isotropy effects on the redistribution term in Reynolds-Averaged Navier-Stokes modelling. *Journal of Fluid Mechanics* **438**, 307–338.

MAYLE, R. & SCHULTZ, A. 1997 The path to predicting bypass transition. *Journal of Turbomachinery* **119**, 405–411.

MENTER, F. 1993 Zonal two equation $k-\omega$ turbulence models for aerodynamic flows. *Tech. Rep.*. Eloret Institute, Sunnyvale, CA.

MENTER, F., KUNTZ, M. & LANGTRY, R. 2003 Ten years of industrial experience with the SST $k-\omega turbulence model$. In *4th Int. Symp. on Turbulence Heat and Mass Transfer*. Antalya, Turkey.

MORAN, A. G. B. 2004 Prediction of the axisymmetric impinging jet with different $k-\varepsilon$ turbulence models. Report 04/29. Dept. of Thermo and Fluid Dynamics, Chalmers University of Technology, G¨oteborg, Sweden, mSc Thesis.

MOSER, R., KIM, J. & MANSOUR, N. 1999 Dns of turbulent channel flow up to $\mathrm{re}_\tau = 590$. *Physics of Fluids* **11**, 943–945.

NARASIMHAMURTHY, V. D. 2004 Unsteady-rans simulation of turbulent trailing-edge flow. Report 04/31. Dept. of Thermo and Fluid Dynamics, Chalmers University of Technology, G¨oteborg, Sweden, mSc Thesis.

NILSSON, H. 2002 Numerical investigations of turbulent flow in water turbines. PhD thesis, Dept. of Thermo and Fluid Dynamics, Chalmers University of Technology, G¨oteborg, Sweden.

OBI, S., AOKI, K. & MASUDA, S. 1993 Experimental and computational study of turbulent separating flow in an asymmetric plane diffuser. In *Ninth Symposium on Turbulent Shear Flows, Kyoto, Japan*, p. 305.

PATEL, C., RODI, W. & SCHEUERER, G. 1985 Turbulence models for near-wall and low Reynolds number flows: A review. *AIAA Journal* **23**, 1308–1319.

PETTERSSON-REIF, B. A. 2000 A nonlinear eddy-viscosity model for near-wall turbulence. AIAA paper 2000-0135.

PHILLIPS, O. M. 1969 Shear-flow turbulence. *Annual Review of Fluid Mechanics* **1**, 245–264.

POPE, S. B. 1975 A more general eddy-viscosity hypothesis. *Journal of Fluid Mechanics* **72**, 331–340.

RADOMSKY, R. 2000 High freestream turbulence studies on a scaled-up stator vane. PhD thesis, University of Wisconsin-Madison.

RADOMSKY, R. & THOLE, K. 2000 Measurements and predictions of a highly turbulent flowfield in a turbine vane passage. *Journal of Fluids Engineering* **122**, 666–676.

RUBENSDÖRFFER, F. 2002 Literature survey: Vane and blade secondary flow and endwall heat transfer. Rept. kth-hpt-37/02. Dept. of Energy Technology, Royal Insitue of Technology, Stockholm.

SHARMA, O. & BUTLER, T. 1987 Predictions of endwall losses and secondary flows in axial flow turbine cascades. *Journal of Turbomachinery* **109**, 229–236.

SIEVERDING, C. 1985 Recent progress in the understanding of basic aspect of secondary flows in turbine blade passages. *Journal of Engineering for Gas Turbines and Power* **107**, 248–257.

SIMONEAU, R. & SIMON, F. 1993 Progress towards understanding and predicting heat transfer in the turbine gas path. *International Journal of Heat and Fluid Flow* **14**, 106–128.

SPENCER, M. & JONES, T. 1996 Endwall heat transfer measurements in an annular cascade of nozzle guide vanes at engine representative Reynolds and Mach numbers. *Journal of Heat and Fluid Flow* **17**, 139–147.

SVENINGSSON, A. 2003 Analysis of the performacne of different $\overline{v^2} - f$ turbulence models in a stator vane passage flow. Licentiate thesis. Dept. of Thermo and Fluid Dynamics, Chalmers University of Technology, Gothenburg, Sweden.

SVENINGSSON, A. & DAVIDSON, L. 2004 Computations of flow field and heat transfer in a stator vane passage using the $\overline{v^2} - f$ turbulence model. In *ASME Turbo Expo 2004*. To appear in conference publication. Vienna, Austria.

SVENINGSSON, A. & DAVIDSON, L. 2005 Computations of flow field and heat transfer in a stator vane passage using the v^2-f turbulence model. *Journal of Turbomachinery* **127**, 627–634.

THOLE, K., RADOMSKY, R., KANG, M. & KOHLI, A. 2002 Elevated freesteam turbulence effects on heat transfer for a gas turbine vane. *International Journal of Heat and Fluid Flow* **23**, 137–147.

VERSTEEG, H. & MALALASEKERA, W. 1995 *An Introduction to Computational Fluid Dynamics*. Addison Wesley Longman Ltd.

WALTERS, D. & LEYLEK, J. 2004 A new model for boundary layer transition using a single-point rans approach. *Journal of Turbomachinery* **126**, 193–202.

WILCOX, D. 1993 *Turbulence Modeling for CFD*. Griffin Printing, Glendale.